CHALMERS
UNIVERSITY OF TECHNOLOGY

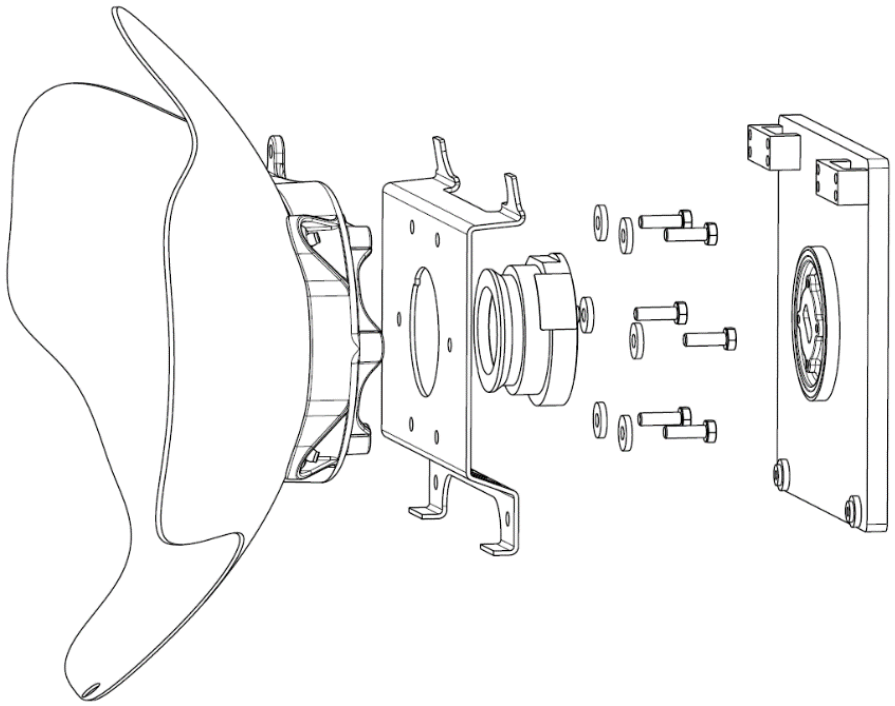

Leakage Reduction by Improved Radio Mounting Design

A product development project focused on reducing RF- and water leakage in outdoor radio units

Master's thesis in Product Development

Jacob Hällgren

Otto Petrén

DEPARTMENT OF INDUSTRIAL AND MATERIALS SCIENCE
DIVISION OF PRODUCT DEVELOPMENT

CHALMERS UNIVERSITY OF TECHNOLOGY

Gothenburg, Sweden 2020
www.chalmers.se

Acknowledgements

Firstly, we would like to thank our supervisors at Ericsson, Henrik Pettersson, *System Mechanical Designer* and Prosha Maaruf, *Mechanical Design Engineer*, for guiding us through the project and giving us valuable input. We would also like to thank our academic supervisor, Göran Gustafsson, *Senior Lecturer at the division of Product Development, Department of Industrial and Materials Science,* for providing meaningful and constructive feedback on our work. Lastly, we would like to thank Malin Oscarsson, *Manager at Mechanical and Thermal Design at Ericsson*, for giving us such a warm welcome and making sure that we had everything we needed in the project.

Abstract

Microwave hops is a technology used to transmit data wirelessly between two separate points in a telecommunications network. The data is transmitted and received with antennas connected to one or multiple radio units. Water and RF-leakage are two factors that are known to negatively affect performance. The project has been executed at the request of *Ericsson AB* and it has had two main focuses. Improving the existing interface between radio unit and antenna with regards to said types of leakage, and investigating and suggesting testing methods that enable objective testing of water leakage, interface force, and interface contact coverage.

The attachment points, which connect the radio to the antenna, and their placement have been analyzed both with regards to rigid body misalignment and contact pressure distribution. The analysis showed that the current attachment point placement can cause low pressures on the side of the interface and that a symmetrical attachment point placement is preferable. A concept generation of alternative mounting mechanisms was performed with the results from the analyses as a base. The generated concepts were evaluated based on cost, assemblability and overall design. The final concept was further developed and a prototype was built to enable comparison with the current design with regards to interface pressure distribution. Pressure sensitive microcapsule films were used to test the concept. The prototype generated a more even pressure distribution compared to the current design with the chosen test method. However, the results indicated that the pressure limit of the film was exceeded, making conclusions regarding prototype performance hard to make.

A literature study of commercially available testing methods was performed. Data of the investigated methods was gathered and compared in order to assess the methods applicability. *Mass flow sensing* was identified as a suitable method for testing water leakage, and three setups of different testing methods for force and contact coverage testing were compiled.

Contents

1 Introduction

The following chapter presents the background to the project and states the project aim. Project limitations and a set of questions intended to specify the investigated issue are presented. Lastly, the report disposition is given.

1.1 Background

Microwave hops are today used as a cost saving alternative to fiber cables as a link between radio towers, in tele-communications networks. The technology uses microwaves to transmit data wirelessly, which is suitable for environments where cable laying is problematic or not optional.

This type of system is affected by several types of disturbances, which is a problem as it can reduce performance for the customers. One type of disturbance and data loss can be attributed to two types of leakage. Water leakage, where water penetrates the interface between the radio unit and the remaining components, which damages the radio equipment, and radio frequency (RF) leakage, where radio waves escape the interface and thereby reduce performance.

This project will be focused on improving the interface by preventing leakage. The studied product consists of five main components; radio, interface plate, transition hub, coupler and reflector. The interface between the transition hub and the radio has one single waveguide port, guiding the radio waves from the radio unit to the reflector. In order to minimize RF leakage and prevent the elements from affecting performance, it is important that the two surfaces of the interface surrounding the waveguide port are correctly aligned after manual assembly by the installer on site. An improved and more robust interface calls for proper and easy alignment of the surfaces in the waveguide interface, which will be the main focus of the project.

The project has been executed at the request of Ericsson, which is one of the largest suppliers of equipment and services used in tele-communications. The company was founded in 1876 and currently has roughly 100 000 employees all over the world.

1.2 Aim

The main goal of this project is to improve the existing interface between the radio unit and the transition hub by eliminating water leakage and preventing RF leakage, while maintaining easy installation.

The project's expected outcome is a CAD-model of the suggested design improvements in STEP format and a prototype that enables testing and comparison with the existing design. Methods for testing water and RF leakage will be investigated, and suitable options be presented.

1.3 Limitations

The following list describes the limitations of the project.

- The project will be focused on a single 13 GHz radio unit configuration and radios of other frequencies will not be considered
- The design space will be limited to the interface plate, radio, and transition hub
- Surface contact and surface force are the sole measurements for measuring RF-leakage
- Methods for testing water leakage, surface contact and force will be investigated and studied but not developed

1.4 Specification of issue under investigation

The issue under investigation is clarified with the following set of questions.

- What factors in the current design cause RF- and water leakage?
- How can the design be improved to eliminate water leakage and prevent RF leakage?
- How does the mounting mechanism affect leakage?
- What methods for testing surface contact, surface force and water leakage are commercially available?

1.5 Disposition of the report

The report mostly follows the chronological order in which the project has been carried out and it is divided in to 10 chapters. Chapter 1 and presents the background to project and its aim and limitations. Chapter 2 gives the needed theoretical background and chapter 3 presents investigated testing methods and the product under investigation in more detail. Chapter 4 details all simulations that were performed to analyze the current design and to understand what aspects affect leakage. All generated concepts are presented in chapter 5 and the concept elimination process is described in chapter 6. The prototype is presented in chapter 7. Lastly, the project is discussed in chapter 8 and concluded in chapter 9. References are presented in chapter 10. Since the report follows a chronological order, results from each phase is presented in their respective chapters.

2 Theoretical Background

The following chapter gives the needed theoretical background in order to understand the remainder of the report. Topics included are general radio wave theory, theoretical background to all software used in the project, leak theory, and force and pressure measurement theory.

2.1 Radio waves and polarization of antennas

Radio wave technology uses electromagnetic waves to transport data wirelessly [1]. This technology is widely used in multiple products, e.g. television, radio, mobile phones, etc. Electromagnetic waves consist of two perpendicular fields, an electric and a magnetic field.

For many radio wave applications it is important that the electromagnetic waves are polarized, meaning that the electric field, *E*, is focused in a certain direction [2]. There are three types of polarized waves, linear, circular and elliptical. The electric field can be divided into two perpendicular electric waves, E_x and E_y. If these are in phase with each other, the resulting electric field fluctuates on a fixed plane in the direction of wave propagation, see Figure 1. In that case the polarization is linear, and the electromagnetic field propagates linearly in the z-direction.

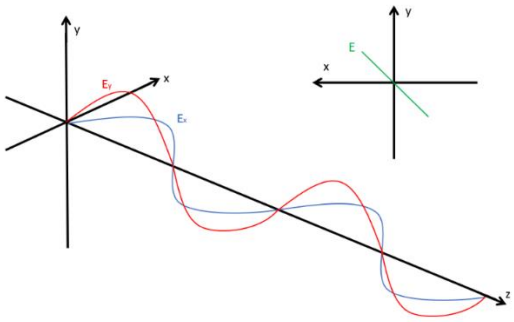

Figure 1: Linear polarization

If the electric waves have a phase offset of $\frac{\pi}{2}$ in relation to each other and equal amplitude, the electromagnetic wave is circularly polarized, see Figure 2. The resulting electric field, *E*, will increase in the z-direction, resembling a circular spiral.

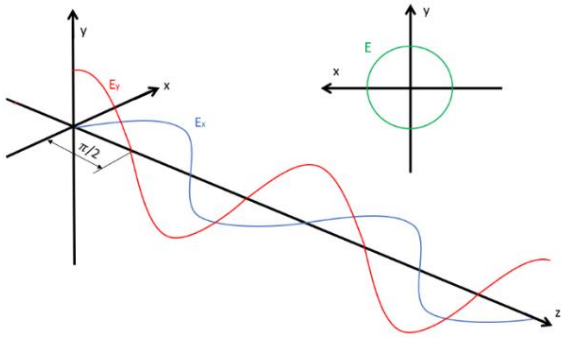

Figure 2: Circular polarization

If the electric waves are arbitrarily positioned in relation to each other, in the direction of the propagation, and have different amplitudes the polarization is elliptical, see Figure 3. The resulting electric field will increase in the z-direction, resembling an elliptical spiral.

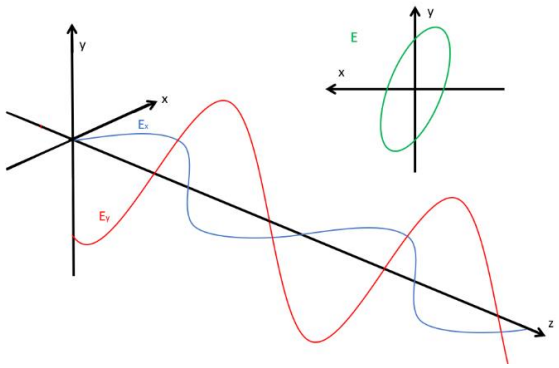

Figure 3: Elliptical polarization

The most common type of polarization used on antennas is linear [3]. This type of configuration often allows a switch between vertical and horizontal linear polarization.

2.2 Line of sight links and hops

Line-of-site links, also called microwave links, is a type of transmission system that uses radio waves to transmit data [4]. This type of system is part of what is called a *transit network* and works as a wireless data link between two points in a tele-communication network. These systems usually operate at a frequency between 400 MHz to 95 GHz. It is important that the line of site is free of obstacles in order for the radio waves to travel between the system connection points without disturbance. If the distance between the two points is far and if there is a lot of uneven terrain the performance of the link can be compromised. In that case, one or multiple “hops” of radio antennas can be added to divide the distance and avoid significant performance drop.

2.3 Hollow RF waveguides

Simply put, a hollow waveguide is a tube with a reflective inside that is used in different applications to guide electromagnetic waves [5]. The shape and size of the cross section affects the wave propagation [6]. Each waveguide has a certain cutoff frequency which depends on its size. Waves cannot propagate in the waveguide if the frequency is below this limit. Some common examples of shapes are rectangular, circular, and squared. Figure 4 shows an example of rectangular hollow waveguide.

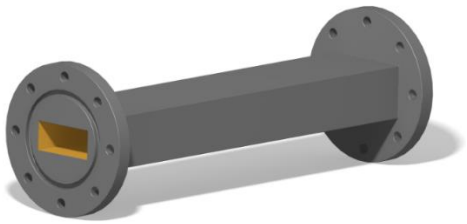

Figure 4: Hollow waveguide

It is important that the inside of the tube is reflective to reduce wave propagation loss [5]. Waveguides often have flanges that able coupling [7]. Seals or gaskets can be used to prevent fluids to enter the coupling. It is common that waveguide flanges are secured with bolts and there is a clear correlation between high bolt torque and low radio wave leakage [6].

2.4 Robust design

The concept of a nominal design exists only in theory and the digital realm. When produced or assembled, a component or product always deviates from the ideal design and thus producing two identical parts is in practice impossible, at least from an economic perspective [8]. This means that every produced product slightly differs from the nominal design. These small geometrical changes are called variation. A robust design is a design which is insensitive to geometrical variation caused by manufacturing and operations [9]. This is often shown with a simple illustration of two different ways of mounting a beam, see Figure 5.

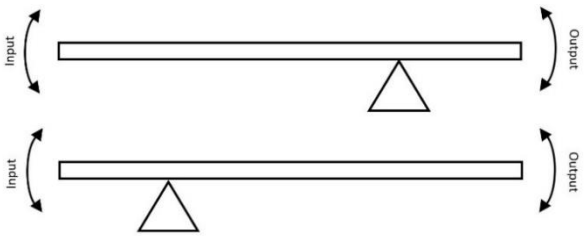

Figure 5: Simplified example of robust design

The first beam is mounted in way that makes small changes in input have large effects on the output, a typical example of a non-robust design. The mounting of the second beam has the effect that large changes in input only marginally changes the output, thus causing little variation, resulting in a robust design.

2.4.1 Tolerances

No product can be produced with perfect accuracy and the physical product will always differ from the nominal design. Tolerances are used to specify how much a certain measurement is allowed to deviate from the nominal design. Tight tolerances are known to come with higher costs, but at the same time, loose tolerances can affect assemblability and functionality [10].

2.4.2 3-2-1 locating schemes

To lock a rigid object in space, all six degrees of freedom, translation along the x-, y- and z-axis and rotation around the x-, y- and z-axis, must be locked. This can be done by implementing a so called 3-2-1 locating scheme [11]. Three primary points A1, A2 and A3 form a base plane that hinders the geometry from rotating around the x- and y-axis and translationally moving along the z-axis, hence three degrees of freedom are locked, see Figure 6.

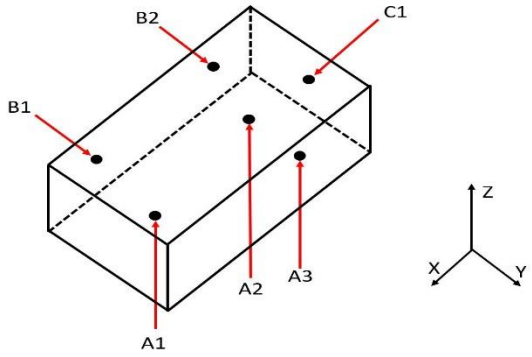

Figure 6: A 3-2-1 locating scheme

The secondary points, B1 and B2, forms a line and locks rotation around the z-axis and translation along the y-axis, locking degree four and five. The last point, C1, locks translation along the x-axis, thus all six degrees of freedom are locked.

2.4.3 RD&T

RD&T, short for Robust Design and Tolerancing, is a software used for analyzing the effects of geometrical variation [12]. It utilizes three main types of analyses to assess robustness and evaluate the given tolerances, Stability analysis, Statistical variation simulation and Contribution analysis [13]. Variation is assessed using three types of measures, *gap*, the horizontal distance between two surfaces, *flush*, the vertical distance between two surfaces and *parallelism*, the angle between

two surfaces. What surfaces or points that are of interest is defined by the user.

Stability analysis

The stability analysis does not consider tolerances and is therefore most useful at an early stage in development. It determines the geometrical sensitivity of a product or component based on the position of a specified number of locators and therefore gives a general assessment of a design's geometrical robustness. The output of the analysis is a 3D-visualization of the product, which indicates where and how variation will occur. After the simulation has been performed, manual or automatic, computer aided optimization of the locator positions can be carried out in order to improve the result.

Statistical variation simulation

The variation is statistically calculated using Monte-Carlo simulations [13]. Necessary tolerances, critical measures and points or surfaces of interest are specified by the user as an input and the normal distribution of variation is calculated for each tolerance. The variation of the tolerances effects how much variation occurs in the points or surfaces in the specified measures and with the tolerance variation, output variation can be calculated. A normal distribution curve is generated for each critical measure and thus the tolerances and their effect on geometrical variation can be studied in detail.

Contribution analysis

The last analysis tool is the contribution analysis. It provides a ranked list of the tolerances and points that contribute to a specified variation, thus highlighting areas of improvement in regard to variation.

2.5 Design for assembly

Design for assembly, DFA, is an engineering tool, that aids the design and engineering process by providing methods and guidelines which aim to ease assembly and thereby lower assembly costs [14]. DFA also provides objective ways of assessing assemblability, which can be used for benchmarking competing products or comparing several concepts at an early stage in development. The concept of DFA was first developed during the 80's when Boothroyd and Dunherst presented a method for analyzing the number of parts effect on assemblability [15]. Since then a large number of alternative academic and industrial methods have been presented and detailed [16].

2.5.1 AviX

AviX is a production optimization software that offers a collection of systematic tools and methods to improve different types of processes [17]. One of these tools can be used for DFA. It allows the user to create a product structure and divide the product into modules. Each module is graded based on predetermined criteria regarding design aspects by following the product assembly process [18]. This generates a score for each module that can be compared between modules to help identify potential areas of improvement. The assembly time is also calculated and can be used for analysis.

2.6 CES Edupack

CES Edupack is a software containing a database of manufacturing methods and materials [19]. The software's purpose is to act as teaching resource in Materials education. The information in the database is structured in different levels, which eases the choice of material and manufacturing methods.

2.7 Finite element method

The finite element method, FEM, is a method used in computational mechanics to solve complex problems [20]. Some common areas of use are structural, fluid and thermal dynamics. Based on a digital model, numerical methods are used to generate a meshed geometry which is built up of elements and nodes. Through a numerical process based on partial differential equations, each element is calculated based on engineering mechanics. All elements are then put together, creating a holistic model and an approximation of the problem domain.

2.7.1 Meshing

The appropriate size and number of the elements depends on the complexity of the problem. An increase of elements generally means greater precision, however, it also means a greater computational demand. The goal is to create a model that is reliable without using unnecessary computing time [20]. This is known as convergence [21].

There are different types element shapes that can be applied to a model [20]. Quadrilateral and hexahedral elements are known to be the most reliable element shapes, these can however be hard to apply on complex geometries. Triangular and tetrahedral shapes are easier to apply and preferred if the geometry is complex.

When creating and evaluating a mesh it is important to consider the element ratio [21]. Figure 7 shows an example of a triangular element with a balanced and an unbalanced element ratio. Unbalanced elements should be avoided to ensure reliable simulation results.

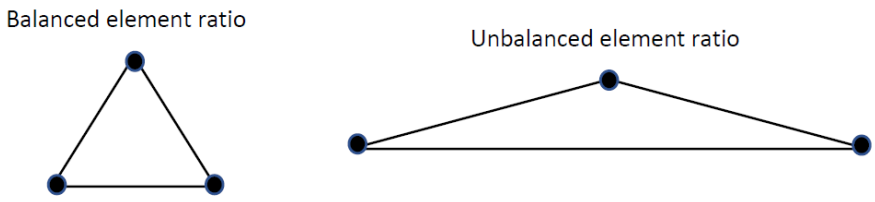

Figure 7: Balanced and unbalanced Element ratio

When simulating a structural mechanics model there will be areas with stress concentrations [21]. High stress concentrations can result in structural failure and it is therefore important that the appropriate type and size of mesh is applied on those areas. This is done by applying local mesh refinements. Some causes of high stress concentrations are sharp edges and different types of cracks and notches.

2.7.2 Ansys workbench & structural mechanics

Ansys is simulation software that offers a variety of different FEM applications [22]. One of these applications is static structural analysis and it is used for structural mechanics. The workflow when using static structural analysis is first to create a model geometry [23]. The type and size of elements are defined together with material properties and then a mesh is created. Boundary conditions are then applied and the desired solution options are chosen. The last step is to run the simulation and evaluate the results.

2.8 Leaks

Leaks are undesirable openings in a product or package, through which solids, gases or liquids can enter or escape [24]. This may result in lowered performance or in the worst case, complete product malfunction. There are many different types of leaks, ranging from the permeation that occurs naturally within the material, to leaks in detachable connections, such as flanges [24]. The severity of the leak depends on the leakage rate, q, in relation to the maximum allowed leakage rate, $MALR$. The leakage rate is the flowrate of a gas or liquid that passes through an opening or openings as a result of a pressure difference between the inner- and the outer environment at a given temperature [25]. It is defined as a rise in pressure in a product with a given internal volume over time, according to equation 1,

$$q = V\frac{\Delta p}{\Delta t} \tag{1}$$

, where Δp is the change in pressure, V is the internal volume of the vessel or product and Δt is the change in time [26]. If a gas is used and the test temperature and the molar mass are known, the mass gas flow ($\dot{m}$) can be calculated according to equation 2,

$$\dot{m} = \frac{\Delta m}{\Delta t} = \frac{qM}{RT} \tag{2}$$

, where Δm is the change in mass in, Δt is the change in time, q is the leakage rate, M is the molar mass, R is the gas constant and T is the temperature [24].

2.9 General theory for force and pressure measurement

When assessing a force or pressure measurement methods applicability, there are a few key

specifications that must be considered in order to get accurate readings [27].
These include nonlinearity, hysteresis, non-repeatability and creep. A theoretically perfect load cell has an output proportional to the load, see dotted line in Figure 8.

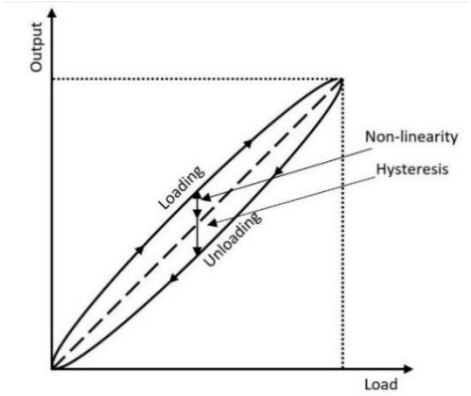

Figure 8: Graph showing hysteresis and non-linearity in relation to a theoretically perfect load cell (dotted line)

In reality this is never the case and the previously mentioned specifications describe in what way and how much the output differs from the theoretically perfect load cell.

Non-linearity

This parameter describes the calibration curves maximum deviation from the dotted curve, see Figure 8, meaning that this parameter describes the cells measurement error over its intended force range.

Hysteresis

Hysteresis is a measurement of how much the output differs between two tests with the same applied load, see Figure 8. The two tests are performed in opposite directions. In the first test, the load increases from zero to its maximum value (loading) and in the second test, the load starts at its maximum and decreases until it reaches zero (unloading). For some applications, hysteresis can be ignored, since only the loading phase is of interest.

Non-repeatability

Non-repeatability describes the maximum difference between outputs for a specific load, see Figure 9. I.e. if a cell is loaded with the same load several times under the same conditions, non-repeatability is a measurement of how large the difference between the outputs are in the worst case.

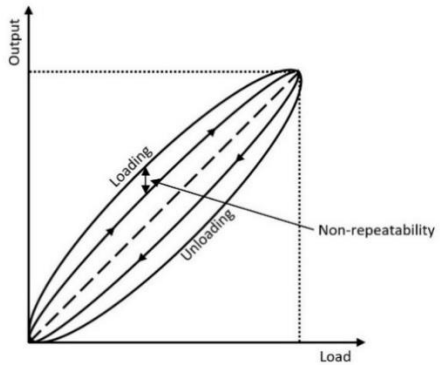

Figure 9: Graph showing non-repeatability in relation to a theoretically perfect load cell

Creep

Creep describes how the output from a load cell load changes over time when conditions are unchanged, and the load is static and does not change.

3 Pre-study

The following chapter describes the current design and explains its functions and assembly process. Identified methods for leakage testing are presented along with identified methods for contact and force testing. All methods are then compared and evaluated, and a recommended leakage testing method and three alternative force and contact measurement setups are presented. Lastly, a requirements list for the product is presented.

3.1 Current design

The investigated product is part of what is called a microwave hop, see Section 2.2. The product consists of a *reflector, coupler*, *interface plate*, *transition hub*, and *radio*, see Figure 10.

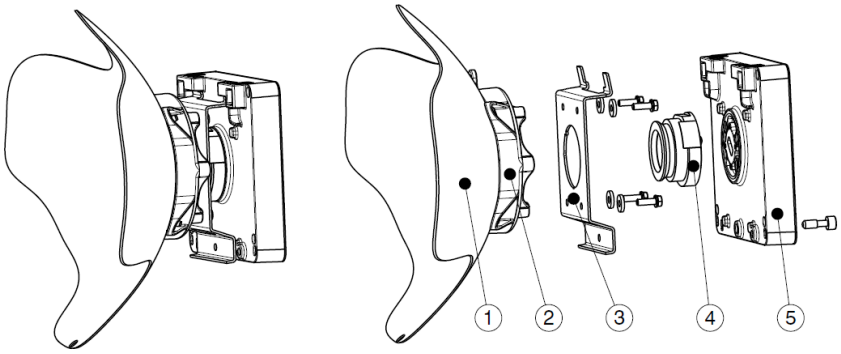

1	Reflector
2	Coupler
3	Interface Plate
4	Transition hub
5	Radio

Figure 10: Product assembly

3.1.1 Product structure

The investigated components are the radio, transition hub, and interface plate. The main purpose of the interface plate is to secure the radio to the coupler, which sits on the backside of the reflector. The interface plate is made of bent sheet steel and has two hooks and a threaded hole intended for a mounting screw, see Figure 11. It also has a circular hole in the middle to make room for the transition hub. The interface plate is secured with four screws to the coupler.

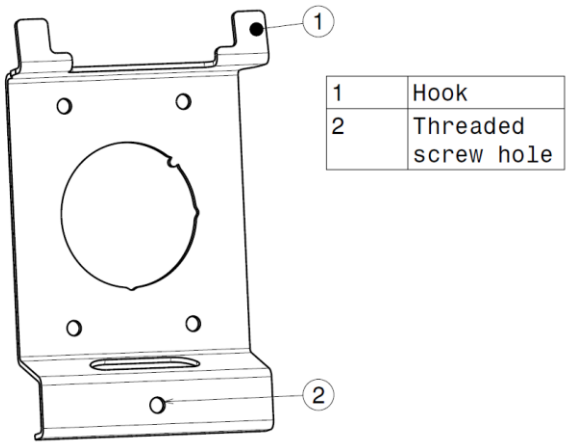

1	Hook
2	Threaded screw hole

Figure 11: Interface plate

The transition hub is used to transfer radio waves between the reflector and radio. It can be divided into the following parts, waveguide cylinder, guiding pins (screws), plate disk, and O-ring, see Figure 12. The cylinder functions as a waveguide and is the main component that all the other components are mounted on. The radio waves pass through a rectangular hole that goes through the entire cylinder. Attached to the top of the cylinder are two screws that functions as guiding pins and as securing mechanisms for the plate disk. The function of plate disk is to help with polarization, and it can be mounted in two different positions, intended for vertical- or horizontal polarization. The screws match with two holes on the radio and helps with port alignment. To prevent water from penetrating the interface between the transition hub and radio, an O-ring is placed in a groove on top of the cylinder.

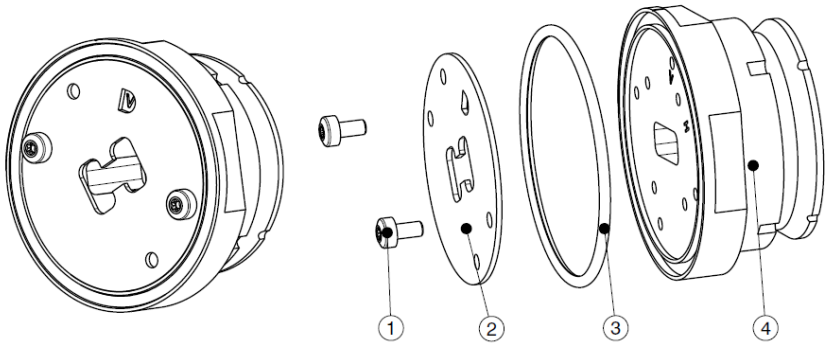

1	Guiding pins
2	Plate disk
3	O-ring
4	Waveguide cylinder

Figure 12: Transition hub and included components in assembled view and exploded view

The radio has two loops intended for the hooks on the interface plate and a screw intended for the mounting screw hole on the interface plate, see Figure 13. The waveguide interface on the radio has a tilted rectangular hole that transfers the radio waves.

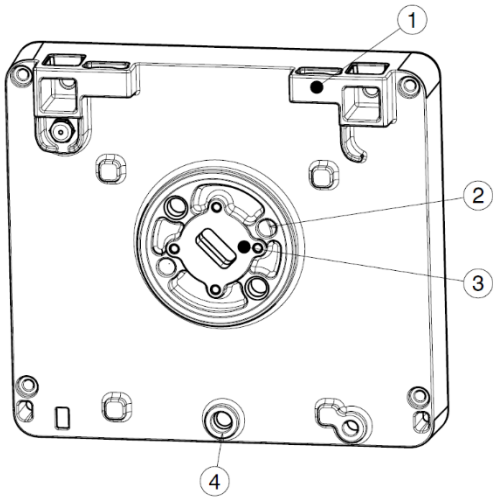

1	Loop
2	Guiding hole
3	Waveguide interface
4	Screw hole

Figure 13: Backside of radio

3.1.2 Assembly instructions

The product assembly process is partially made at the production site and partially made by the installer on site. The interface plate is pre-mounted at the production site with four screws and washers to the coupler. The transition hub and its components are pre-assembled. At site, it is pressed on to the coupler, fitted in the center hole of the interface plate. It can be placed in two different positions, with the waveguide port in vertical or horizontal direction. To switch from vertical to horizontal polarization or vice versa, the transition hub is removed and rotated 90 degrees around its central axis. In vertical polarization, the rectangular waveguide port on the waveguide cylinder is vertically aligned. In horizontal polarization, the waveguide port on the waveguide cylinder is horizontally aligned. The plate disk has two different mounting positions, one for vertical and one for horizontal polarization, meaning that it has to be unscrewed and reattached if polarity is switched. After the transition hub has been mounted, the radio is hung on to the radio interface plate, see marker A in Figure 14, and secured with a screw using a T-handle hex key. As the screw is tightened, the interface plate starts deforming. The deformation causes reaction forces at the attachment points of the radio, which in turn creates pressure in the waveguide interface. This whole process is carried out on the ground. The entire setup is then secured to a pole on the radio tower with the mounting kit.

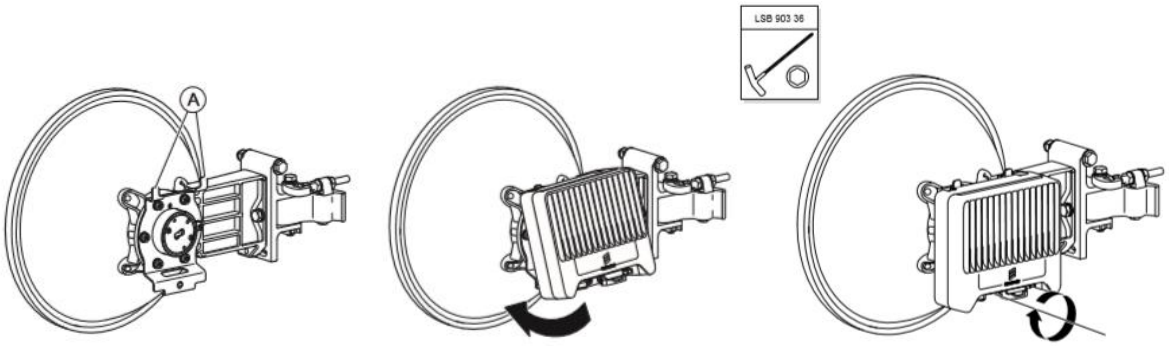

Figure 14: Radio installation procedure, here pictured with an alternative interface plate

3.2 Leak testing methods

A leak test can have two main purposes, locating the leak by identifying the point of entry or exit and quantifying the leak by measuring the leakage rate [24]. When deciding on a leak testing method for a specific product, the flow direction of the leak should preferably be considered. A leak testing method should reflect the products actual application, i.e. if a product is prone to inwards leaking a test method for inwards leaking should be chosen and vice versa [24]. Nasa has categorized leak test methods based on the leak flow direction into five categories, *total external-to-internal, total internal-to-external*, *total internal-to-internal*, *local internal-to-external* and *local external-to-internal* [25].

Total external-to-internal

The combined flow of all tested leaks has an inward direction, from the outside to the inside of the tested product. This type of leak testing is often called outside-in leak testing.

Total internal-to-external

The combined flow of all tested leaks has an outward direction, from the inside to the outside of the tested product. This type of leak testing is often called inside-out leak testing.

Total internal-to-internal

These methods test for leaks that occur within the tested product. The leak flows from one compartment of the product to another.

Local internal-to-external

This type of leak testing method, tests for inside-out leaks at a specific point or part of the product.

Local external-to-internal

This type of leak testing method, tests for outside-in leaks at a specific point or part of the product.

In the case of the studied product, there is no pressure difference between the inside and outside of the product. The leak flow direction is inwards, since the purpose of the seals is to keep water from penetrating the product and damaging its components. For said reason, only external-to-internal leak testing methods will be investigated and presented. However, most methods are applicable for testing both inside-out and outside-in leaks. Even though leakage quantification is the primary purpose when testing the radio assembly, the number of potential entry points is fairly large, hence suitable methods for leakage detection have also been studied.

3.2.1 Pressure rise / Vacuum decay technique

The pressure rise method is built on the principle that gases flow from a point of higher pressure to a point of lower pressure. By making the internal pressure of a hollow product lower than the surrounding pressure, one can make a gas flow from the surrounding environment into the product if there is an opening that lets the gas penetrate the product. The tested product is evacuated, which means that the

pressure within the product is lower than the pressure outside of the product. Figure 15 shows a simplified layout of the pressure rise method.

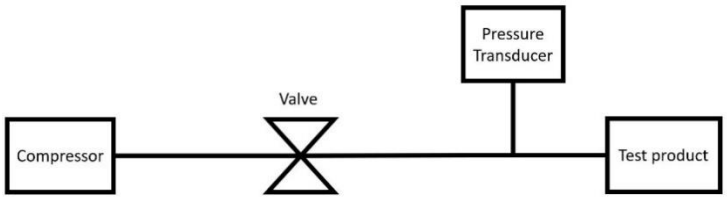

Figure 15: Simplified layout of the pressure rise method

If the product is leaking, the surrounding media will penetrate the product and the internal pressure will increase. The method is carried out according to the following step-by-step process [24].

1. A pump evacuates the product and after the evacuation of the internal gases is complete, the pump valve is shut. The internal pressure difference, ΔP_1 is measured over a period of time, ΔT_1.
2. The valve is then opened, and the pump is run a second time in a similar fashion and once again, the internal pressure difference, ΔP_2 is measured over a time period, ΔT_2.
3. The pressure change for the two runs is then studied. If the test product is not completely sealed, alternatives, *a*, *b* and *c*, are possible, see Figure 16.
    a. The pressure increase is constant during both runs, meaning that the pressure increase per time unit is unchanged throughout the test. This indicates that a leak is present.
    b. The pressure increase slowly tapers off and finally reaches zero. This indicates that gas could have been liberated from the walls of the product during the first run.
    c. A combination of the two prior bullet points is observed.

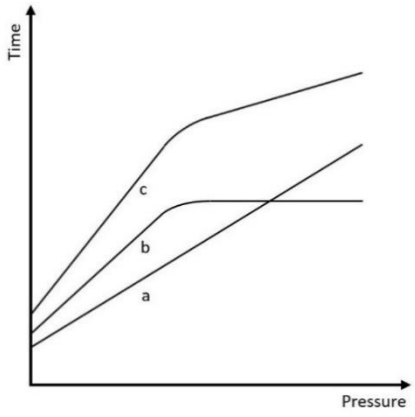

Figure 16: Alternative outcomes when using vacuum decay [24].

Once alternative b and c have been ruled out and it is clear that a leak is present, equation 1 in section 2.8 can be used to calculate the leakage rate.

The maximum sensitivity of the method varies between $\frac{10^{-3} mbar*l}{s}$ to $\frac{10^{-5} mbar*l}{s}$ depending on manufacturer and technology implementation [25], [28].

3.2.2 Mass flow sensing / Mass extraction

Mass flow sensing share many similarities with the pressure rise method. The test part is evacuated (or pressurized) but the gas flow is not shut like in the pressure rise method. Instead, the test part is held at a certain internal pressure by pumping in or out gas to or from the test part and the mass flow of gas needed to maintain said pressure is measured by a flow meter, see Figure 17.

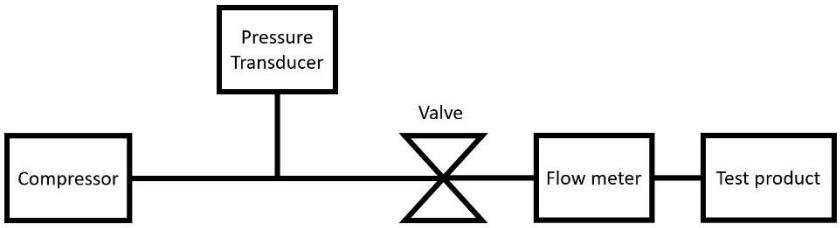

Figure 17: Simplified layout of the mass flow sensing method

This means that the actual leakage rate is measured directly, and no unit conversion or calculation is necessary [29]. Since the actual leakage rate is measured, no calibration when switching between test products is necessary. The maximum sensitivity of the method varies between $\frac{10^{-2} mbar*l}{s}$ to $\frac{10^{-4} mbar*l}{s}$ depending on manufacturer and technology implementation [30], [31].

3.2.3 Tracer gas-based methods

Tracer gas-based methods measure leakage rate by measuring the concentration of a gas that either leaks in or out of the tested product. The most commonly used gas is helium since it has small molecules, which makes detection of very small leaks possible [28]. Helium is also a non-toxic, inert gas that exists only in small concentrations in air, meaning that the risk for non-reliable test results and damage to the operator is fairly low [32]. To measure the helium concentration mass spectrometers are used.

Hood / Enclosure test / Outside-in Leak Testing

The hood method shares many similarities with the pressure rise method but its main way of measuring the leakage rate differs. The test product is placed in a chamber, a hood, which is filled with a tracer gas, often helium [33]. The test product is then evacuated and a tracer gas detector (mass spectrometer), placed in the vacuum line, measures the amount of helium in the gas that is being evacuated from the products inside, see Figure 18.

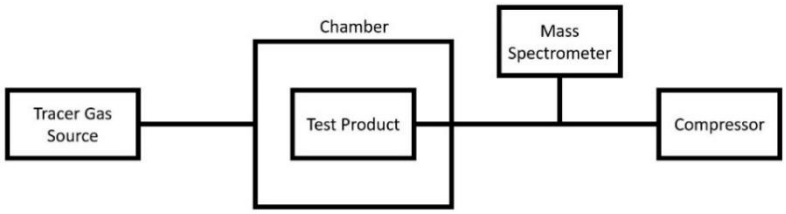

Figure 18: Simplified layout of the hood method

The method has a very high maximum sensitivity between $\frac{10^{-6}mbar*l}{s}$ to $\frac{10^{-11}mbar*l}{s}$ but it cannot identify the location of the leak, since the entire product is tested at once [33], [28].

Vacuum spray test / Tracer probe method

The vacuum spray test is a method primarily used for identifying local outside-in leaks [24]. The test product is evacuated, and a mass spectrometer or other gas detector is placed in the vacuum line. A fine spray gas is then slowly applied around all seals, flanges and other potential leakage points of the product [34]. If a leak is present, the helium will penetrate the opening, causing the tracer gas detector to detect it, see Figure 19.

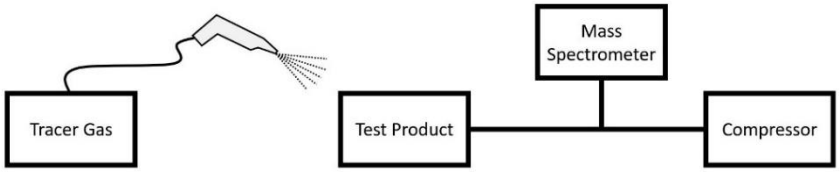

Figure 19: Simplified layout of the vacuum spray test method

The method is fully manual, and its performance is dependent on the skill and experience of the operator using the spray [24]. It is classed as semi-quantitative since it measures the leakage rate but it only does so on a local level [25]. The maximum sensitivity of the method varies between $\frac{10^{-6}mbar*l}{s}$ to $\frac{10^{-8}mbar*l}{s}$ [28], [25].

3.2.4 Leak testing methods comparison and verdict

The current requirement on leakage is given as a maximum allowed volume flow in $\frac{ml}{minute}$, see Appendix *A: Product requirements specification*, meaning that unit conversion is necessary to obtain the maximum allowed leakage rate, $MALR$, which industry standard unit is $\frac{mbar*l}{s}$. To convert a volume flow ($\dot{v}$) to a mass flow ($\dot{m}$), which is needed to calculate the $MALR$, multiplication with the material density, ρ, is necessary, see equation 3.

$$\dot{m}_{max} = \dot{v}_{max}\rho \tag{3}$$

The radio is not filled with any specific gas and it is mounted outside, meaning that the gas that flows in and out of potential leaks is air. With the density of air, ρ_{air}, and the maximum allowed volume flow, $\dot{v_{max}}$, the maximum allowed mass flow, $\dot{m}_{max}$, is calculated according to equation 4, 5 and 6.

$$\dot{v}_{max} = 5\frac{ml}{minute} = 8.33 * 10^{-8}\frac{m^3}{s} \tag{4}$$

$$\rho_{air,298K} = 1.184\frac{kg}{m^3} \tag{5}$$

$$\dot{m}_{max} = 8.33 * 10^{-8} \frac{m^3}{s} * 1.184 \frac{kg}{m^3} = 9.863 * 10^{-8} \frac{kg}{s} \quad (6)$$

With a known mass flow, $MALR$ can be calculated by rearranging equation 2 in section 2.8, to the following formula, see equation 7, 8, 9, 10 and 11.

$$R = 8.314 \frac{\mathrm{J}}{mol * K} \quad (7)$$

$$M_{air} = 0.029 \frac{kg}{mol} \quad (8)$$

$$T_{Test\ env} \approx 298\mathrm{K} \quad (9)$$

$$q = \frac{RT\dot{m}}{M} \quad (10)$$

$$MALR = \frac{8.314 * 298 * 1.02 * 10^{-7}}{0.029} = 0.00843 \frac{J}{s} = 8.43 * 10^{-5} \frac{bar * l}{s} = 8.43 * 10^{-2} \frac{mbar * l}{s} \quad (11)$$

In order to detect leaks that have a leakage rate equal to the $MALR$, the leak testing method needs to have a sufficient sensitivity. The sensitivity of the different methods varies greatly, depending on manufacturer and the implementation of each technology. In the bar chart below, see Figure 20, the maximum sensitivity for all four identified leak testing methods are presented. Since data has been gathered from a large number of sources, the maximum sensitivity is given as a span, rather than a specific number. The chart also includes a line, which represents the $MALR$ of the radio, meaning that all methods with a maximum sensitivity to the right of the line are able to detect leaks smaller than the $MALR$.

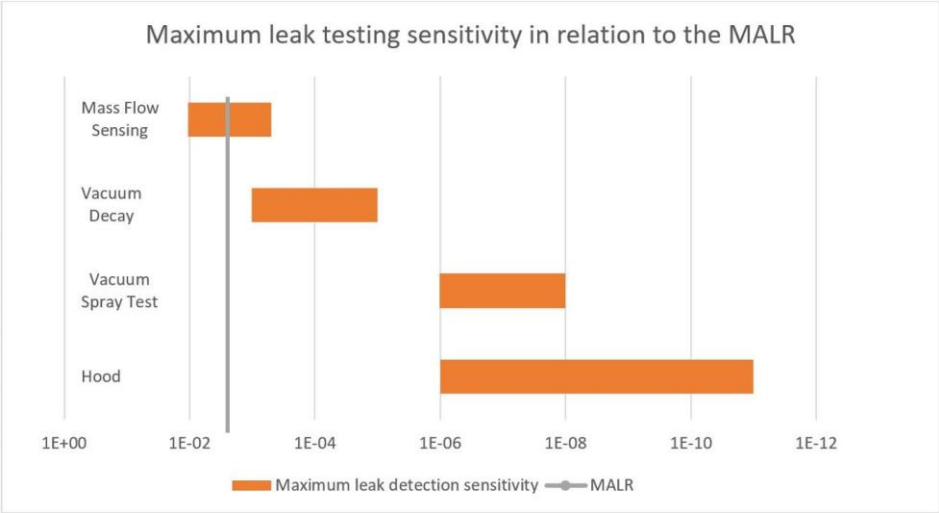

Figure 20:Maximum leak testing sensitivity in relation to the maximum allowed leakage rate

All presented methods are therefore viable options if one only considers the method sensitivity. Mass flow sensing's maximum sensitivity is close to the $MALR$ but the method is still believed to be suitable, considering the large variety of manufacturers available on the market. Cost is highly dependent on manufacturer, but the following table gives a rough estimate of the cost for each method, see Table 1.

Table 1: Cost estimates for the identified leak testing methods [35].

	Mass flow sensing	**Vacuum Decay**	**Vacuum Spray Test**	**Hood**
Cost estimate (USD)	5000	7500	25 000	80 000

The vacuum spray test is not a suitable option since it cannot quantify the total leakage rate, but it could act as a compliment to other leakage methods. However, it comes at a substantial cost and is therefore not preferable for the purpose of testing the product. The hood method is very sensitive but considering the relatively high $MALR$, it is not a suitable option, since it is the highest priced method that has been investigated. Pressure rise and Mass flow sensing are priced relatively equal to each other and have similar sensitivities. The vacuum decay method is built on equation 1 in section 2.8, meaning that the internal volume of the tested product, V, affects the result. Every time a component or product with a different internal volume is tested, the machine must be recalibrated [29]. Since mass flow sensing measures the actual leakage rate, no calibration is necessary when switching between test products with different internal volumes. Since, there are small variations of the internal volume in reflectors from different suppliers, mass flow sensing is a preferable method.

3.3 Contact testing methods

In the following section, the only identified method for contact testing will be presented. In section 3.5, methods for surface pressure testing will be presented. These could be used as methods for contact testing as well and should therefore be viewed as alternatives to the method presented in this section.

3.3.1 Ink testing

The ink tests primary purpose is to test mating between two surfaces. A thin layer of dye is applied manually on one of the surfaces using a brush. The amount of dye, the layer height and the area it is applied on varies depending on the operator applying the dye. The tested product is then assembled according to the assembly instructions. The two surfaces meet and where there is contact, an imprint from the ink is left on the previously uncolored surface. After disassembly, the ink imprint is analyzed.

3.4 Force testing methods

If the force requirement is met, see Appendix *A: Product requirements specification*, a force of 1400N ±600N should act on surfaces of the waveguide interface and the maximum force acting on the entire interface is roughly 2300 N since the O-ring absorbs around 300 N. To make sure that the contact surface force is within the requirement limits, a method for validating the actual force is needed. The following section present different methods for testing the contact surface force and analyzing their applicability as testing methods. Three categories of force testing methods have been identified, *strain gauge compression load cells, piezoelectric compression load cells* and *piezoresistive force sensors*. All measure force directly, and no unit conversion is necessary. In section 3.5, methods for testing pressure will be discussed. These methods could also act as force testing methods, which will be further discussed in section 3.6. The intended force range and performance specifications differs widely within each of the categories depending on how different companies have implemented the technology. For said reason, alternative manufacturers and specifications for their products have been listed. Another important distinction to make is that all load cell-based methods require a testing rig that mimics the product to work, since it is not possible to place them between the surfaces of the waveguide interface due to their size. This means that the performance and cost of the test setup is dependent on the rig. For said reason, only one commercially available option for the load cell-based technologies will be listed as a reference for price and accuracy.

3.4.1 Strain gauge compression load cells

Load cells are devices used for measuring force and torque. The cells can have many types of sensing elements, but the most commonly used ones are strain gauges [36]. Strain gauges work by measuring the change in electrical resistance caused by the deformation of a spring element built into the cell.

When an object is put under a mechanical load, F, it either expands or contracts, which is called Poisson's effect [37]. The load causes a stress, σ, in the the object according to equation 12,

$$\sigma = \frac{F}{A} \tag{12}$$

where A is the area F acts upon. This causes the object to deform and the ratio between the deformation and the initial dimensions of the object is called strain, ε, and is defined according to equation 13,

$$\varepsilon = \frac{L_2 - L_1}{L_1} = \frac{\Delta L}{L_1} \tag{13}$$

where L_2 is the length of the object after deformation, L_1 is the length of the object before deformation and ΔL is the deformation length [38]. How much the object deforms depends on the Youngs modulus, E, of the material according to Hookes law, see equation 14.

$$\sigma = E\varepsilon \tag{14}$$

Poisson's ratio, v, describes the ratio of longitudinal (x-axis) and transversal (y-axis) strain, according to the following formula, see equation 15,

$$-\frac{\varepsilon_T}{\varepsilon_L} = v \tag{15}$$

where ε_T is the transversal strain and ε_L is the longitudinal strain [36]. If a material is deformed within its elastic range, it has a proportional stress response to the applied strain [39]. If the strain is larger than the elastic range tolerates, the spring element will deform plastically and the cell will not work as intended [36]. Hence, the spring material needs to be chosen with care. By rewriting Ohm's law, electrical resistance, R, can be written according to equation, see equation 16,

$$R = \rho\frac{l}{A} \tag{16}$$

where ρ is the electrical resistivity of the material, l is the length of object and A is the cross-sectional area [36]. Since l and A change during deformation, the electrical resistance is proportional to the strain. This can then be used to form the Gauge Factor, GF, which relates the change in resistance to the change in strain according the following equation, see equation 17,

$$GF = \frac{\Delta R L_1}{R \Delta L} = \frac{\Delta R}{R\varepsilon} \tag{17}$$

where ΔR is the resistance after deformation and R is the resistance before deformation [38]. To measure the actual change in resistance a Wheatstone Bridge is used. The bridge is a type of electrical circuit that can detect small changes in resistance, by measuring the output voltage of the circuit [40]. Hence, the force that acts on the load cell can be measured.

Futek LTH300

Futek LTH300 is a series of donut-shaped compression strain gauge load cells with a maximum capacity from 222 to 4448 N [41]. The sensor itself is priced at 830 EUR [42]. In order to use it, it needs to be connected to a signal processing unit that can display the forces the sensor measures.
For reference, Rinstrum N320, is a signal processing unit which can be connected to Futeks loadcells and it is priced at 4000 SEK [43]. The load cell's performance specifications are listed in Table 2.

Table 2: Futek LTH300 load cell performance specifications [41].

Non-linearity	±0.5%
Non-repeatability	±0.5%
Hysteresis	±0.5%

3.4.2 Piezoelectric compression load cells

A piezoelectric material is a crystalline material, that when put under a mechanical load exhibits the piezoelectric effect, meaning that an electric charge is produced when a load is applied [44]. Piezoelectric force sensors consist of three layers, see Figure 21.

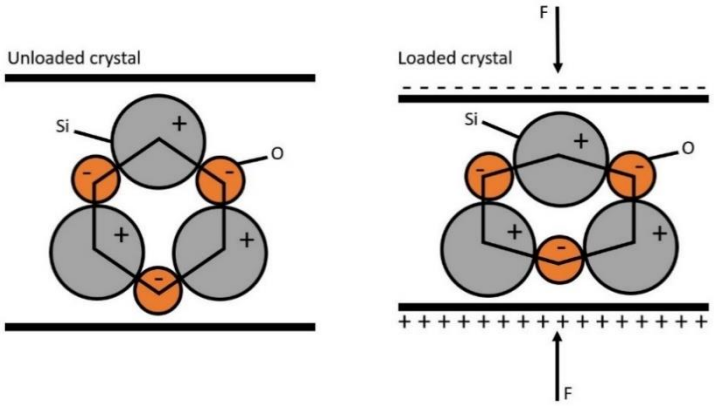

Figure 21: Example of a piezoelectric sensor with a quartz middle layer

The middle layer is made of a piezoelectric material with area A and thickness t [45]. The load causes a strain in the material, which in turn causes an electric charge, $\pm Q$, at the electrodes (top and bottom layer) proportional to the size of the load, F, according to equation 18,

$$\varphi = \frac{Q}{C} \approx \frac{dF}{C} = \frac{d}{4\pi\varepsilon_r} \frac{tF}{\varepsilon_0 A} \tag{18}$$

, where C is the static capacitance of the material, d is the piezoelectric constant of the material dependent on the crystal structure, ε_r is the relative dielectric constant of the middle layer, ε_0 is the permittivity of vacuum and φ is the electric potential caused by the charge [45]. Commonly used materials include quartz, tourmaline and ferroelectric ceramics [46].

Kistler SlimLine Sensor 9132B

SlimLine is a series of piezoelectric load cells intended for measuring compressive dynamic forces [47]. The cells have a maximum capacity ranging from 2.5-80 kN. In order to get the system operational, a signal processing unit is needed [48]. Performance specifications for 9132B can be seen in Table 3: Performance specifications for 9132B . No data regarding price has been found.

Table 3: Performance specifications for 9132B [47]

Non-linearity	<±1%
Hysteresis	<1%

3.4.3 Piezoresistive force sensors

Materials that exhibit the piezoresistive effect when put under a mechanical load, meaning that their electrical resistance change as they are deformed, are called piezoresistive materials or piezoresistors [49]. The materials used in this type of sensors utilizing this effect varies extensively from conductive rubber, conductive polymers and polymer films, conductive gels, conductive fibers and yarns to pressure sensitive ink [45]. For force testing purposes, this type of sensor is often called a Force sensing resistor or FSR. When no mechanical load is applied on the FSR, the resistance is very high (hundreds of kiloohms), and as the load is applied, the resistance drops to few kiloohms [50].

FSR UX 406 by Interlink Electronics

FSR UX 406 is a sensor in the FSR UX 400-series develop by Interlink Electronics [51]. Of all FSRs Interlink produces it has the widest force sensing range and it can detect forces between 0.5 N and 150 N. The sensing area is 34*34 mm and thickness is 0.46 mm. The sensors performance specifications are listed in Table 4.

Table 4: FSR UX 406 performance specifications [51].

Non-repeatability (Single part)	±2%
Non-repeatability (Part to part)	±5%
Hysteresis	±5%
Creep (5kg, 10 days)	<4% log10 (time)

The sensor itself is priced at 5 USD, however this cost does not include all other needed equipment to perform force tests [52].

FlexiForce A502 by TekScan

FlexiForce A502 is the largest standard force sensing resistor in the FlexiForce series [53]. The sensing area measures 50.8*50.8 mm and it has a thickness of 0.203 mm [54]. It is flexible and has a standard measurement range of 0-222N, but it can measure forces up to 44 448 N if a lower drive voltage is applied [54]. The sensors are sold in packs of four and one package is priced at roughly 110 USD [54]. In order to use the sensor TekScans FlexiForce OEM Development Kit is needed. It is priced at 370 USD [55]. The sensors performance specifications are listed in Table 5. TekScan also delivers sensors of custom dimensions.

Table 5: FlexiForce A502 performance specifications [54].

Non-linearity	<±3%
Non-repeatability	<±2.5%
Hysteresis	<±4.5%
Creep per log time	<±5%

Tactilus by Sensor Products Inc.

Tactilus is a measurement system that works with piezoresistive sensors intended for either direct force measurement or pressure measurement. The system is developed by Sensor Products Inc. and is compatible with a large variety of sensors [56]. Of the sensors intended for direct force measurement, the two sensors with the largest area are SP011 and SP013, see Table 6.

Table 6: Tactilus force sensing resistors specifications [56].

Sensor	**Dimensions (mm)**	**Thickness (mm)**	**Pressure range (MPa)**	**Force range (N)**
SP011	25 in diameter	0.25	0 - 1.379	0 - 491
SP013	25*25	0.25	0 - 1.379	0-625

The cost of a Tactilus system starts at a price of 5000 USD [57]. Performance specifications are listed in Table 7.

Table 7: Tactilus system performance specifications [58].

Non-repeatability	±2%
Non-linearity	±1.5%
Hysteresis	±5%

3.5 Pressure testing methods

The following section presents and details alternative solutions for testing surface pressure in the interface. All presented methods primary purpose is to test and analyze contact pressure between mated surfaces, but they are believed to be valid options for testing force and surface contact coverage as well. Five main categories of technologies have been identified. The intended pressure range in which

the technologies are applicable, and the thickness of the actual device used to measure the pressure differs widely within each of the categories depending on how different companies have implemented the technology. For said reason, alternative manufacturers and specifications for their products have been listed for each investigated technology. For some technologies, only one commercially available solution was found.

3.5.1 Capacitive pressure sensors

This type of sensor estimates the applied pressure by measuring the change in capacitance, C [46]. The sensors have three main layers, a bottom and a top layer constructed by conductive plates, and a middle layer of a compressible dielectric material, see Figure 22.

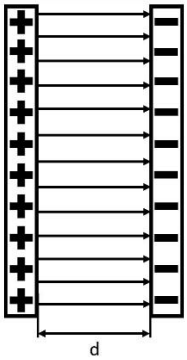

Figure 22: Capacitive sensor layout [59].

As pressure is applied on the upper conductive plate, the middle layer gets compressed, which causes the capacitance to change, in accordance with equation 19,

$$C = 4\pi\varepsilon_r\varepsilon_0\frac{A}{d} + C_f \tag{19}$$

, where d is the distance between the plates, ε_r is the relative dielectric constant of the middle layer, A is the area of the plates, ε_0 is the permittivity of vacuum and C_f is the capacity contribution from the edges of the electrodes [45]. To get more than one sensing point, capacitive pressure sensors can be placed in a matrix pattern, which creates an array. Each crossing in the array becomes a sensing point, a sensel, see Figure 23 [59].

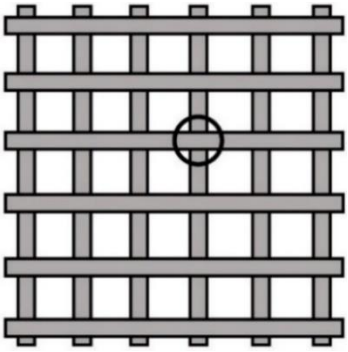

Figure 23: Sensel, marked by circle

Industrial Tact Array System

Pressure Profile has developed a capacitive sensor system called Industrial TactArray [60]. The systems sensors are 0.3 mm thick, can withstand moderate bending and the intended pressure range is 0-4.826 MPa [61]. System performance specifications are listed in Table 8.

Table 8: Tact Array system performance specifications [61].

Non-linearity	±2%
Non-repeatability	±0.4%

Pricing starts at 10 000 EUR which includes sensors, needed electronics and software (Pressure profile systems, personal communication, May 2020).

3.5.2 Pressurex micro green

Pressurex micro green is the brand name of a pressure sensitive film. It consists of two layers, a donor- and a receiver layer. The donor layer is covered in pigmented particles that are chemically attracted to the surface of the receiver layer [62]. When pressure is applied and the two layers meet, a chemical bond between the particles and the coating on the receiver layer forms. During separation, pigment particles from the donor sheet leave an imprint on the receiver sheet, which can be analyzed. The color density in the imprint indicates pressure concentration with an accuracy of ± 17%. The pressure range is 0.007 MPa to 24.821 MPa and the film has a thickness of roughly 0.2 mm. The film comes in five different pressure ranges, see Table 9, and rolls are priced at 500 USD a piece [63].

Table 9: Pressurex Micro Green film types

Film type	**Pressure range (MPa)**	**Roll dimensions (mm)**
PMG 1	0.007 - 0.345	270*3000
PMG 2	0.172 - 0.689	270*6000
PMG 3	0.345 - 3.103	270*6000
PMG 4	1.999 - 10.342	270*12 000
PMG 5	2.413 - 24.821	270*12 000

3.5.3 Piezoresistive Pressure Sensors

These sensors work is the same fashion as piezoresistive force sensors but are made of interlaced lines of a piezoresistive material that form the columns and rows of a matrix [64]. Each crossing in the matrix becomes a sensel, and the resolution is therefore given by the number of columns and rows in the matrix [65].

Tactilus by Sensor Products Inc.

Tactilus is compatible with piezoresistive pressure and force sensors. The sensor thickness and pressure range vary with the dimensions. Two of the sensors intended for pressure measurement and their specifications are listed in Table 10.

Table 10: Pressure sensors for Tactilus [56].

Sensor	Dimensions (mm)	Thickness (mm)	Resolution (sensels/square cm)	Pressure range (MPa)
SP001	25.4*25.4	0.36	36.7	0 - 1.034
SP002	50.8*50.8	0.36	36.7	0 - 1.034

For system performance specifications and price, see section 3.4.3.

I-Scan Evolution by TekScan

The I-scan Evolution system is a pressure sensing system that utilizes piezoresistive matrix sensors for analyzing contact pressure. The system can use different types of sensors intended for different use cases and therefore sensor dimensions and pressure ranges vary extensively [64]. For the intended purpose, the following sensors, 5040, 5051, 5076 and 5051 have been identified and their specifications are listed below, see Table 11.

Table 11:Pressure sensors for I-scan Evolution (TekScan, 2020), (TekScan, 2020), (TekScan, 2020), (TekScan, 2020).

Sensor	Dimensions (mm)	Thickness (mm)	Resolution (sensel/square cm)	Pressure range (MPa)
5040	44.7*44.7	0.102	96.9	0-3.447
5051	55.9*55.9	0.102	62.0	0-172.39
5076	83.8*83.8	0.102	27.6	0-103.421
5101	111.8*111.8	0.102	15.5	0-34.474

The systems typical performance specifications listed below, see Table 12.

Table 12: I-Scan Evolution performance specifications [66].

Non-linearity	<±3%
Non-repeatability	<±3.5%
Hysteresis	<±4.5%
Creep per log time	<±5%

The entire system, including two sensors, software and all needed equipment for data acquisition is priced at 270 000 SEK (Camat Systems, personal communication, May 2020).

3.5.4 Microcapsule films

Microcapsule films are plastic films developed for measuring contact pressure between two mated surfaces. The film has three main layers, a base PET layer, a color-forming layer covered in micro capsules filled with dye and a color developing layer [67]. The film is cut to shape and then inserted between the surfaces. When pressure is applied the micro capsules burst and leave a colored imprint on the color forming layer. After disassembly, the imprint can be studied, and the density of the color

indicates pressure level. The films come with a reference chart, which allows for visual evaluation, but sellers often provide a software that analyzes scanned imprints with higher precision. The films show peak pressure during the assembly process. After analysis, the imprints are discarded, and the product cannot be reused. The thickness of the film varies between manufacturers, but it is usually between 0.1-0.3 mm.

Prescale by Fujifilm

Fujifilm Prescale comes in eight variants, which are intended for different pressure spans [68]. Span one to five, extreme low pressure to medium pressure, are intended for a pressure range of 0.05 MPa to 50 MPa and use a two-sheet type of film. Span six to eight are used for pressures between 50 MPa – 300 MPa and use a mono layer film. The film thickness varies with the pressure spans, the mono sheet films are approximately 0.11 mm thick and two sheet films are 0.18 mm thick. Under specified conditions, Fujifilm guarantees ±10% accuracy. Each roll is priced around 4200 SEK per piece [69]. The recommended scanner and needed software are priced at roughly 25 000 SEK (Camat Systems, personal communication, February 2020). Table 13 presents all film types that Fujifilm currently offers.

Table 13: Fujifilm Prescale film types [68]

Film type	**Pressure range (MPa)**	**Sheet type**	**Roll dimensions (mm)**
Extreme low pressure (4LW)	0.05 - 0.2	Dual layer	310*3000
Ultra super low pressure (LLLW)	0.2 - 0.6	Dual layer	270*5000
Super low pressure (LLW)	0.5 - 2.5	Dual layer	270*6000
Low pressure (LW)	2.5 - 10	Dual layer	270*10 000
Medium pressure (MW)	10 - 50	Dual layer	270*10 000
Medium pressure (MS)	10 - 50	Single layer	270*10 000
High pressure (HS)	50 - 130	Single layer	270*10 000
Super high pressure (HHS)	130 - 300	Single layer	270*10 000

Surface Profiler by Sensor Products Inc.

Surface Profiler Film is the brand name of microcapsule film developed by Sensor Products Inc. The thickness varies between 0.1 to 0.2 mm depending on the intended pressure span [70]. It comes in five pressure ranges, ranging from 0.055 MPa to 9.65 MPa and Sensor Products specifies an accuracy of ±10%. Rolls of films are priced at around 700 USD a piece and no software is available [71]. Table 14 presents all film types that Sensor Products offer.

Table 14: Surface Profiler film types [71]

Film type	Pressure range (MPa)	Roll dimensions (mm)
SPF-A	0.055 - 0.172	310*3000
SPF-B	0.138 - 0.621	270*5000
SPF-C-LR	0.621 - 2.620	270*6000
SPF-C-ER	0.621 - 9.653	270*6000
SPF-D	2.413 - 9.653	270*12 000

3.6 Force, pressure and contact testing method comparison

In the following sections, requirements for force, pressure and contact testing methods will be detailed and discussed. A short analysis of the investigated methods and three potential testing setups, A, B and C will be presented.

3.6.1 Force and contact testing method requirements

The suggested method or combination of methods primary purposes can be summarized as follows:

- Accurately measure the force that acts on the waveguide interface and accurately measure the force that acts on the O-ring.
- Accurately and objectively measure the contact area in the interface, both on the waveguide interface and the O-ring.

The following requirements list, see Table 15, has been compiled and quantifies the previously defined primary purposes into general requirements for the force and contact testing methods. The requirement list is intended for either one method or a combination of several methods. Some of the identified methods have the ability to perform both contact and force testing simultaneously, while other methods can only perform one of the two tasks.

Table 15: General requirements list for force and contact testing methods

Criteria	Value	Explanation
Force testing		
1. The testing method(s) shall be able to measure a force of 1.5 times the maximum allowed force.	(1400+600+300)*1.5 N = 3450 N	Errors in manufacturing can lead to parts that create forces that are larger than the maximum allowed force.
2. The testing method(s) shall withstand a force of 2 times the maximum allowed force.	(1400+600+300)*2 N =4600 N	Errors in manufacturing can lead to parts that create forces that are larger than the maximum allowed force.

3. The testing method(s) shall be able to measure the force on the waveguide surface and on the O-ring.	Binary (Yes/No)	The force is distributed over both the O-ring and the waveguide surface.
Contact testing		
1. The testing method(s) shall provide objective contact measurement.	Binary (Yes/No)	Subjective interpretations of the result can create misleading results.
2. The testing method(s) shall be operator independent.	Binary (Yes/No)	Human error can create misleading results.
3. The testing method(s) shall be able to measure contact on the waveguide surface and on the O-ring.	Binary (Yes/No)	The contact is distributed over the O-ring and the waveguide surface.
Pressure testing (only applicable to pressure testing methods)		
1. The testing method(s) shall be able to measure a pressure of 1.5 times the maximum pressure.	25*1.5 MPa=37.5 MPa	Errors in manufacturing or assembly can lead to parts that create pressure that are larger than the maximum pressure observed in section 4.1.2.
2. The testing method(s) shall withstand a pressure of 2 times the maximum pressure.	25*2 MPa= 50 MPa	Errors in manufacturing or assembly can lead to parts that create pressure that are larger than the maximum pressure observed in section 4.1.2.

3.6.2 Force, pressure and contact testing method analysis and verdict

To ease the analysis, the methods have been categorized as follows. In each category, the investigated methods applicability in relation to the requirements list will be discussed.

Pressure testing methods for force measurement

All pressure sensitive films, microcapsule films and Pressurex Micro Green, are intended for specific non-overlapping intervals. None of the films has a pressure range that covers the entire span of 0-25 MPa that was measured in section 4.1.2, meaning that if these were to be used as a force measurement method, the entire force that acts on the interface would not be possible to measure. Hence, the films are not valid options for force measurement. Of the remaining methods for pressure testing, only one of the piezoresistive pressure sensors, I-Scan Evolution by TekScan, has a pressure range that covers the entire span of 0-25 MPa, meaning that it is the only pressure measurement method that works for force testing. The range of I-Scan Evolution also covers 50 MPa, which is the maximum pressure requirement.

Direct Force measurement

Of the investigated testing methods intended for direct force measurement, piezoelectric and strain gauge load cells fulfill the force requirements and are therefore valid options. Of the piezoresistive force sensors, the only solution that withstands the force requirement is FlexiForce A502 by TekScan. The sensor is large enough to cover the entire waveguide surface but the corners of the sensors will be in contact with the bulge on the radio-side intended for creating pressure on the O-ring, see Figure 24. The sensor footprint is marked in green and the bulge is marked in orange.

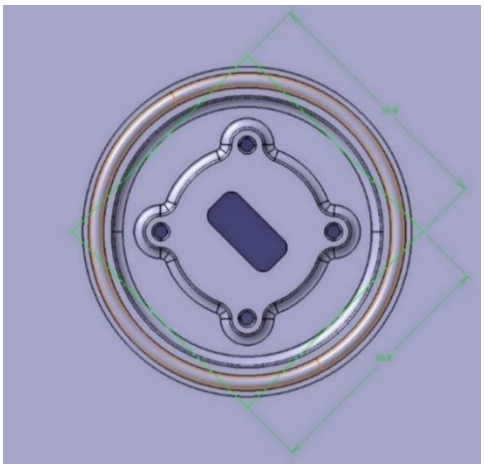

Figure 24: FlexiForce A502 dimensions in relation to the interface on the radio side

This means that two sensors of custom dimensions would have to be used, one that covers the entire interface including the O-ring and one that only covers the waveguide interface.

Contact measurement

Ink testing is highly operator dependent and assessing the results in an objective manner is problematic. The amount of applied dye affects the thickness of the dye layer, which creates uncertainties in the testing methods reliability, hence it does not fulfill the requirements. All the pressure films are valid options for contact testing if a pressure limit that is classified as contact is set. Of the remaining pressure testing methods only piezoresistive pressure sensors, I-Scan Evolution by TekScan, are a valid option, since the rest of them do not withstand the pressure in the waveguide interface.

Testing method setups

Three testing method setups fulfill the general requirements.

A. A piezoresistive pressure sensor used for both force and contact measurement (I-Scan Evolution).
B. A microcapsule film or Pressurex Micro Green for contact measurement and a strain gauge or piezoelectric load cell rig for force measurement.
C. A microcapsule film or Pressurex Micro Green for contact measurement and piezoresistive force sensors for force measurement.

These will be further discussed in more detail and will be referred to as setup A, B and C.

Setup A

The sensors of the I-Scan Evolution are 0.102 mm thick, meaning that the thickness of the actual sensors would have a small effect on the contact testing result compared to most other investigated methods. Sensor 5076 has a large area, which is preferable since force and contact can be measured over both the waveguide interface and the O-ring simultaneously. This means that there is no need to switch sensor between runs, which could change the loading conditions and thus altering the results. Neither is there a need for a test rig, since the sensor is placed between the surfaces of the actual interface. The sensor is bendable but not foldable, meaning that the guiding pins would have to be removed prior testing.

Setup B

No software is needed when using the pressure sensitive films as a contact testing method, hence all pressure sensitive films are deemed to be valid options for contact testing. The thinner the film is, the better the results reflect reality, since less material is added between the surfaces of the interface. The thickness of all investigated films is roughly the same, meaning that in that regard, their performance is similar. The main difference between the identified films is their accuracy when measuring pressure. Since a pressure limit, which is classified as contact, has to be set in order to use these films for testing, their accuracy will carry over to contact testing as well, meaning that the films accuracy will affect the results. Therefore, both invested microcapsule films would be the most suitable options of the pressure sensitive films for contact testing. The guiding pins do not have to be removed when using the microcapsule films, since they can be cut into shape.

The load cells are by far the most accurate of the investigated force testing methods. However, since all load-cells require a testing rig, due to the fact that they cannot be placed between the surfaces of the actual interface, assessing their actual accuracy is problematic. Both piezoelectric load cells and strain gauge-based load cell have a low non-linearity but this does not include the measurement error from the rig.

Setup C

The difference between setup B and C is the way force is measured. Setup C uses two force sensing resistors of custom dimensions from the FlexiForce series. Since the force on the O-ring and the force on the waveguide surface cannot be measured simultaneously, two force tests have to be carried out which can cause measurement errors due to changed loading conditions. The sensor is bendable but not foldable, meaning that the guiding pins would have to be removed prior testing.

Setup cost comparison

The exact cost of each setup is not known but Table 16 presents a rough cost estimate for the three alternatives. All values have been rounded to the closest 10.000 SEK.

Table 16: Approximate setup costs

Setup	**Cost (SEK)**
A	270.000
B	30.000
C	10.000

Prices given in EUR or USD, in previous sections, have been converted with exchange rates of 05-05-2020 (1 USD=9.82 SEK, 1 EUR=10.66SEK). For setup B, the price of one roll of Fujifilm Prescale, one Futek LTH300 and one Rinstrum N320 has been used. The rig needed in setup B has been estimated to a cost of 10.000 SEK. In setup C the cost consists of one roll of Fujifilm Prescale, one FlexiForce OEM Development and a pack of four A502 sensors to represent the two custom sensors needed.

3.7 Product requirement specification

A requirements specification for the product design was compiled based on the pre-study and requirements given by Ericsson. The specification can be found in Appendix *A: Product requirements specification*.

4 Physical Testing and Simulations

The following chapter details and presents the simulations and physical tests that have been performed in the project. The effect the applied torque on the mounting screw has on the waveguide interface force is tested and presented. The pressure range and distribution in the waveguide interface is analyzed and detailed. Furthermore, all performed simulations, both regarding contact pressure and rigid body misalignment, are presented. Lastly, the results from the physical tests are compared to the results from the simulations.

4.1 Physical testing

The physical testing was performed in two stages. Firstly, the force in the interface was tested with different amounts of torque applied on the mounting screw, to see if the applied torque had any effect of the force in the waveguide interface. The second test was performed to establish the pressure range and distribution in the waveguide interface.

4.1.1 Torque test

The effect of the torque applied on the mounting screw was tested with the current force testing rig. The purpose of this was to identify the influence that the applied torque had on the force in the waveguide interface. Three different torques where tested. Since a t-handle hex tool is used to mount the radio there is no recommendation regarding applied torque. To identify a suitable torque range, a t-handle hex tool was used to tighten the screw with hand force. A torque wrench was then used, and torque was slowly applied until the screw started rotating and at this point the torque readout was read. After several tries, a torque range of 10 – 18 Nm was specified. Three values within the range, 10 Nm, 14 Nm and 18 Nm were picked and three tests for each of the values were performed to reduce the potential for error. All torque tests were performed with and without the O-ring attached.

Torque test results

The mean results from the torque test can be seen in Table 17. The mean force generated on the interface, with the O-ring, differed with 5 % at most (the highest force divided with the lowest force), meaning that the applied torque has a small effect on the force in the interface.

Table 17: Torque test results, mean values

Applied Torque (Nm)	Force mean with O-ring (N)	Force mean without O-ring (N)
10	1385	1665
14	1373	1696
18	1456	1661

Results from all torque testing can be found in Appendix *B: Torque tests*.

4.1.2 Film test on current design

In order to assess the pressure range on the waveguide interface, a test kit of Fujifilm Prescale was used. The kit included samples of pressure films for LLLW, LLW, LW, MS, HS and HHS, see section 3.5.4 for pressure ranges. All films were tested, and all the scanned imprints can be seen in Appendix *C: Fuji Film contact test*. The HHS and HS films came out without an imprint, meaning that the maximum pressure on the waveguide surface is lower than 50 MPa, which was expected. The MS-film had a small imprint, left by the edges of the waveguide interface, which suggests that the maximum pressure exceeds 10 MPa. When comparing the imprint on the MS film to the Prescale reference chart, it could be concluded that the maximum pressure is approximately 25 MPa, suggesting that the pressure range is 0-25 MPa.

By comparing the a theoretically perfect imprint, see Figure 25, and the pressure film imprints, see imprint samples in Figure 26, it is clear that the top and bottom of the interface experience higher a pressure than the sides.

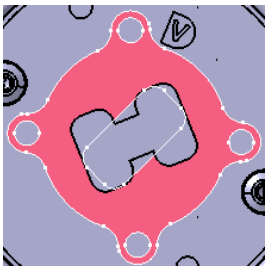

Figure 25: Theoretically perfect imprint

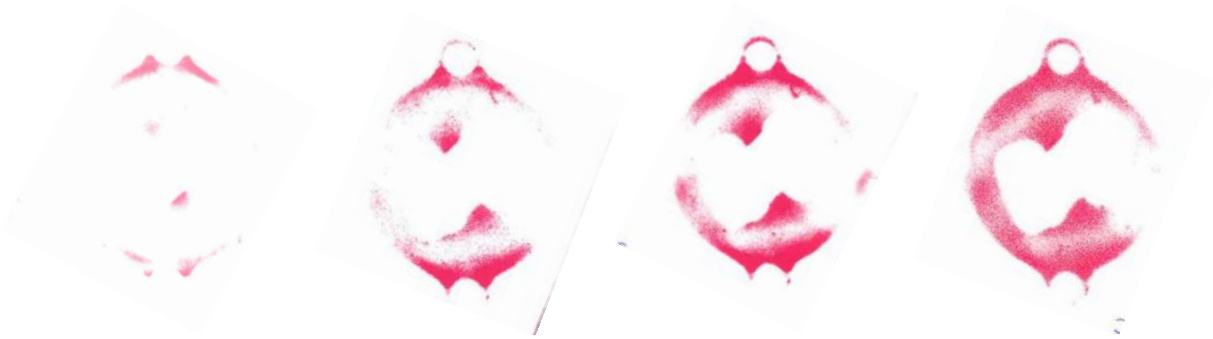

Figure 26: Pressure Film imprints from MS, LW, LLW and LLLW films

The positioning of the attachment points, marked with red circles, in relation to the interface can be seen in Figure 27. The red rings mark the attachment points and the white lined geometry on the transition hub shows the opposing waveguide interface.

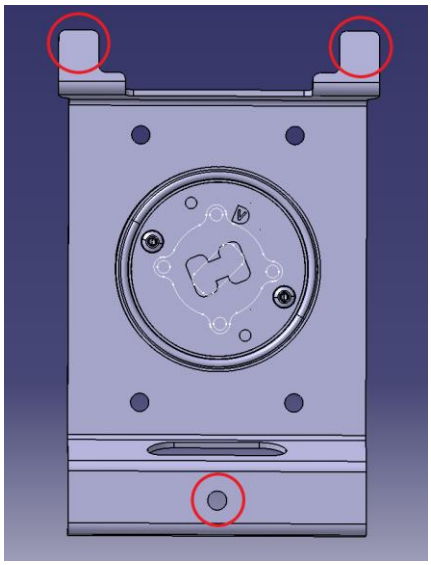

Figure 27: Attachment points in relation to waveguide interface marked in white

No pressure testing was performed on the O-ring, since the sample films were too small to cover the entire O-ring. However, parts of the O-ring were covered by the film, see Appendix *C: Fuji Film contact test*. In all tests, the part of the O-ring that was tested left an imprint with lower color density than that of the waveguide interface, suggesting that the pressure on the O-ring is lower than on the waveguide interface.

4.2 Simulations

Simulations were made to evaluate different configurations of attachment points, including the attachment point configuration of the current design. The position and number of attachment points were analyzed with regards to interface surface pressure and rigid body misalignment.

4.2.1 Simulation of contact pressure in Ansys

A simplified assembly model, representing the radio and transition hub interface was used to reduce computing time. The results are not exact, meaning that they do not fully reflect reality, but they give an indication of how the attachment point placement and number affect contact pressure. Two parameters were investigated: *number of attachment points*, two, three and four; and *distance of attachment points* from the interface center, 40 mm, 80 mm, and 120 mm. Combining these generated a total of 9 different models to be tested. Figure 28 shows three examples of the simplified radio and transition hub assembly used in the simulations (distance from the center to the attachment points is 80 mm).

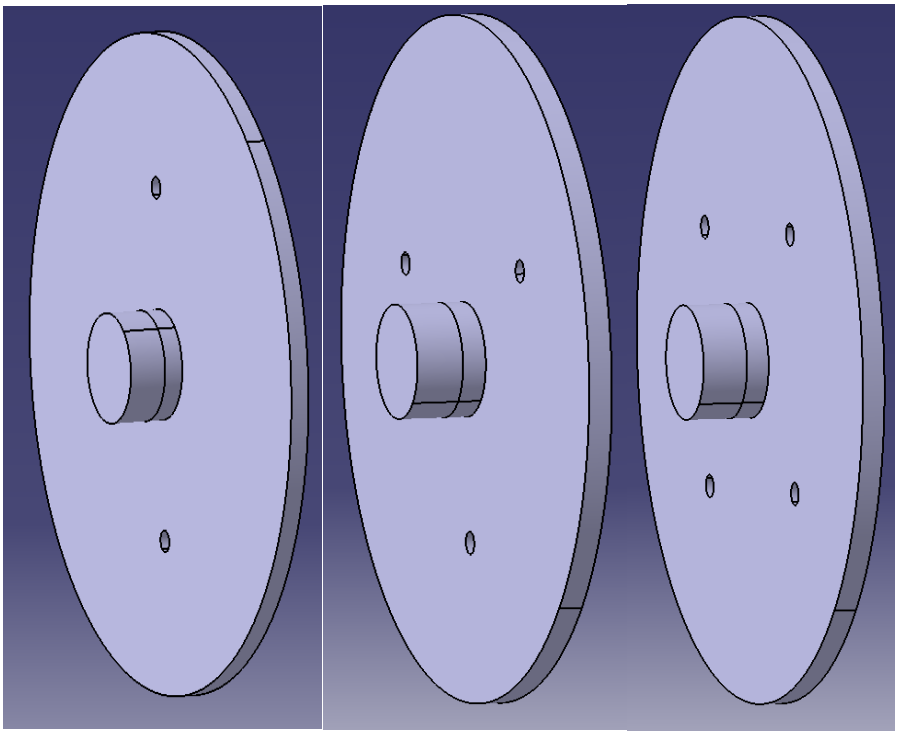

Figure 28: Examples of models used in contact pressure simulations

Each assembly model consisted of two parts, a cylindrical plate (300 mm in diameter) with a smaller cylinder in the center representing the radio side of the waveguide interface, and a mated cylinder representing the transition hub, see Figure 28. The mated surfaces had a diameter of 25 mm. Both parts were assigned the material, structural steel. Each plate had holes representing the attachment points. The holes were used to place the forces. Each model had a force sum of 1200 N evenly distributed amongst the attachment points. A fixed support constraint was assigned to the bottom surface of the transition hub cylinder to secure the model in space. Figure 29 shows an example of the placement of forces and the fixed support. Convergence was reached with a mesh size of 3 mm.

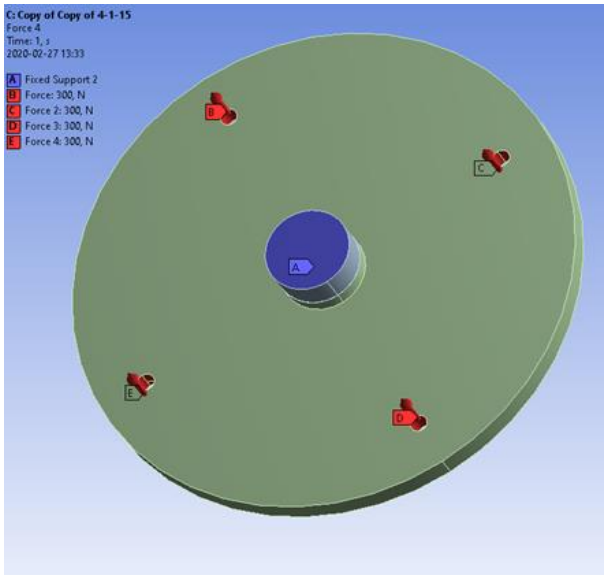

Figure 29: Example of placement of forces and fixed support

Nodal data of the surface pressure in the interface was extracted and saved after each simulation. The percentage of nodes that exceeded a certain pressure limit was calculated for each case, to ease comparison of the results from the different runs. Three pressure limits were tested, 0, 0.2, and 0.4 MPa, to increase the reliability of the results.

4.2.2 Results from Simulation of interface pressure in Ansys

The results for all three pressure limits can be seen in Appendix *D: Contact pressure simulation tests*. A general pattern regarding the two parameters was identified. The percentage of nodes that exceeds the limits was increased as the attachment points were positioned closer to the center of the interface. The same pattern was observed as the number of attachment points was increased. When tabulating the nodal data, it became evident that the difference between three and four attachment points was small, compared to the difference between two and three attachment points, see Figure 30.

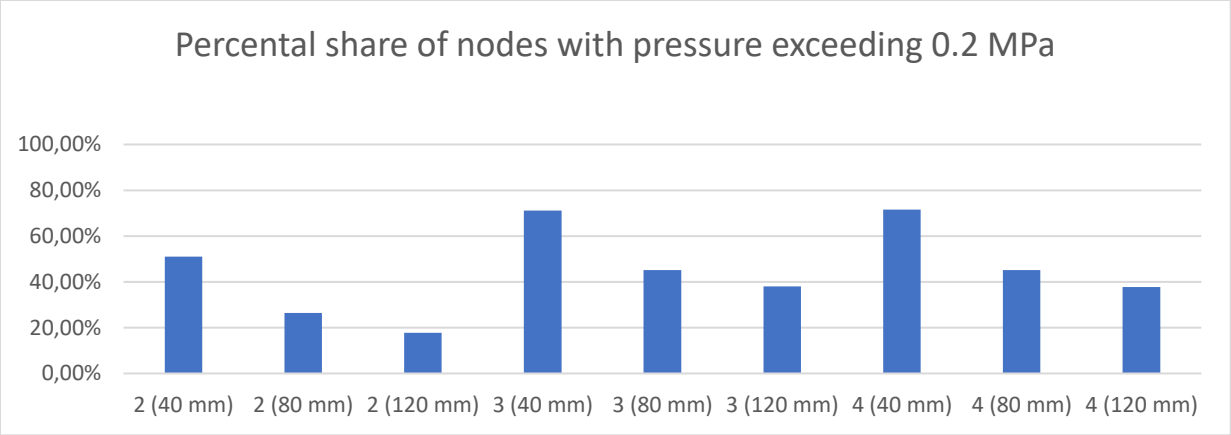

Figure 30: Share of nodes with pressure exceeding 0.2 MPa

Unlike the models with three and four attachment points, the models with two attachment points all had a horizontal path in the center, out to the edges, that experienced very low pressures, see Figure 31. The conclusion is that two attachment points are unsuitable.

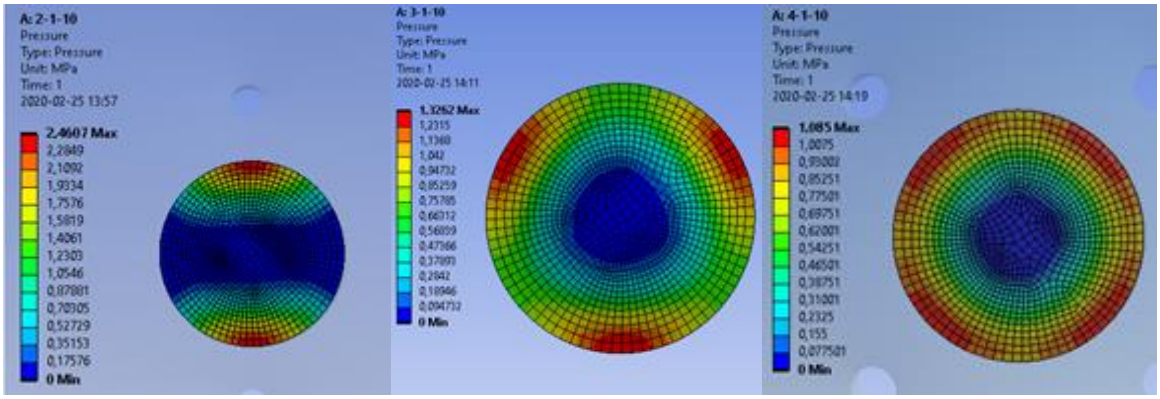

Figure 31: Pressure distribution with two, three and four attachment points at a distance of 40 mm from the interface center.

4.2.3 Attachment points placement effect rigid body misalignment

One of the believed reasons for uneven pressure distribution in the interface is rigid body misalignment, meaning that the actual position of the radio differs slightly from its nominal position, due to tolerances in the attachment points on the radio. This could potentially generate unparallel surfaces in the waveguide interface. To test how the attachment points distance from the center of the interface affects rigid body misalignment, the software RD&T was used.

A model with seven combinations of attachment points was created. The analysis was limited to three attachment points due to that RD&T only handles three attachment points since the software uses rigid bodies. All combinations had three attachment points, symmetrically placed around the interface, see Figure 32.

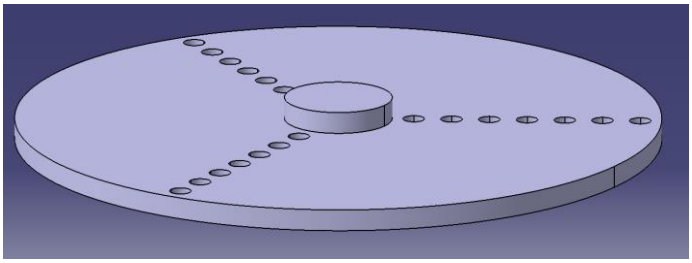

Figure 32: Model used for analyzing rigid body misalignment.

The distances from the interface center at which the attachment points were placed were 35 mm, 52.5 mm, 70 mm, 87.5 mm, 105 mm, 122.5 mm, and 140 mm respectively. For each simulation, the part was fixed with a 3-2-1 positioning system and a linear z-tolerance of ± 0.2 mm was placed on each attachment point, see Figure 33.

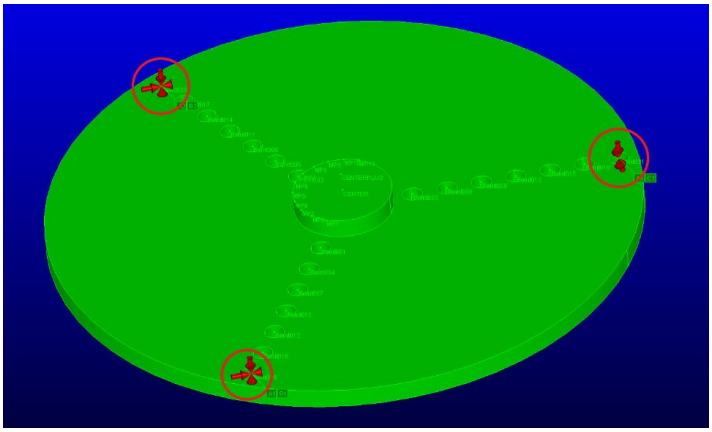

Figure 33: Example of 3-2-1 positioning system marked with red circles.

11 angle measurements were created from the center point of the interface to its edge, see Figure 34. A variation analysis with 1 000 000 Monte Carlo simulations was performed, and the worst-case angle range of the 11 measurements were saved.

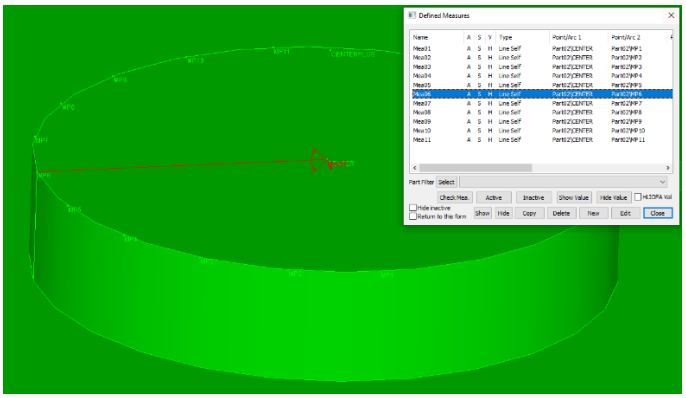

Figure 34: Angle measurements in the interface.

4.2.4 Simulation results from rigid body misalignment analysis

Figure 35 shows the angle range in degrees for the worst of the 11 angle measurements for each of the seven tested combinations of attachment points. The further away from the interface center the points are placed, the smaller the angle range becomes.

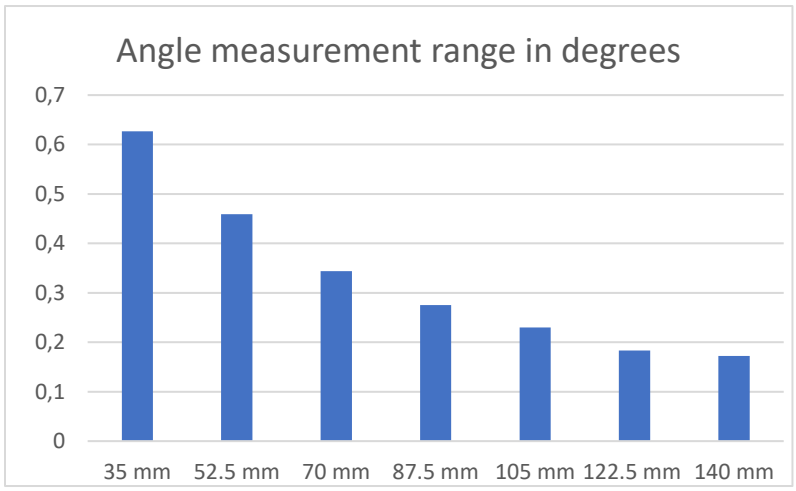

Figure 35: Angle range for the worst angle measurement caused by misalignment.

4.2.5 Rigid body misalignment comparison with the current design

The attachment points of the current design, see Figure 27, were analyzed in a similar fashion as the attachment point combinations in section 4.2.3. A simplified radio with three holes representing the attachment points of the current design was created and given a 3-2-1 locating scheme, see Figure 36.

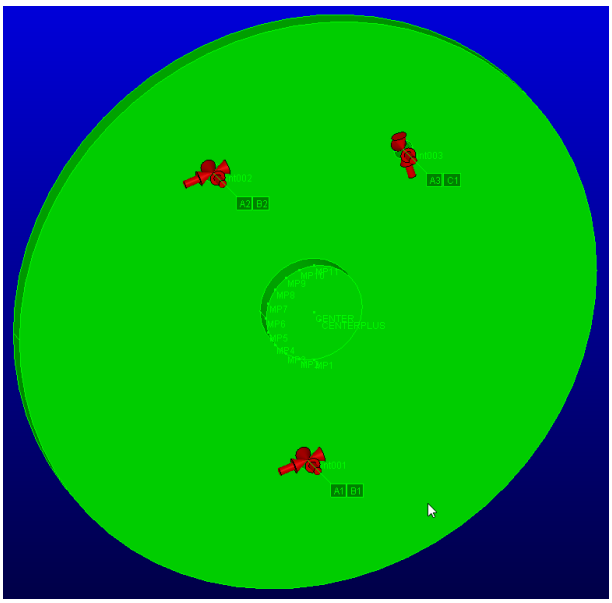

Figure 36: RD&T-model with attachment points from the current design

Each attachment point was given a linear z-tolerance of ±0.2 mm. 1 000 000 Monte Carlo simulations were performed in a variation analysis. The worst angle measurement was 0.408 degrees and appeared at MP6, see Figure 37.

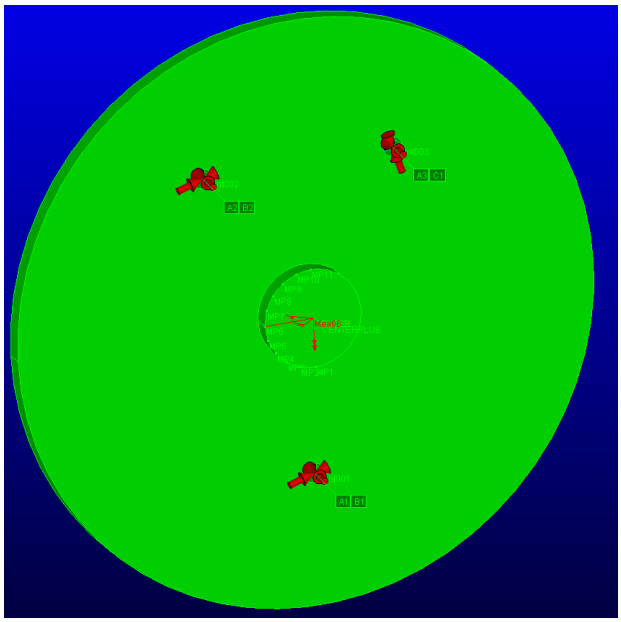

Figure 37: Worst angle measurement marked in red

The attachment points of the current design are not placed at an equal distance from the center of the interface, the bottom point is closer to the center than the two top ones. The bottom point is placed roughly 80 mm from the interface center and the top points are placed roughly 90 mm from the interface center. In section 4.2.4, the attachment points distance from the center of the interface effect on rigid body misalignment was shown. The closer to the interface center the points were placed, the worse results. In Figure 38, the angle measurement range of the attachment points from the current design is compared to the angle measurement range of two combinations of symmetrically placed attachment points, placed at a distance from the interface center of 70 and 87.5 mm respectively.

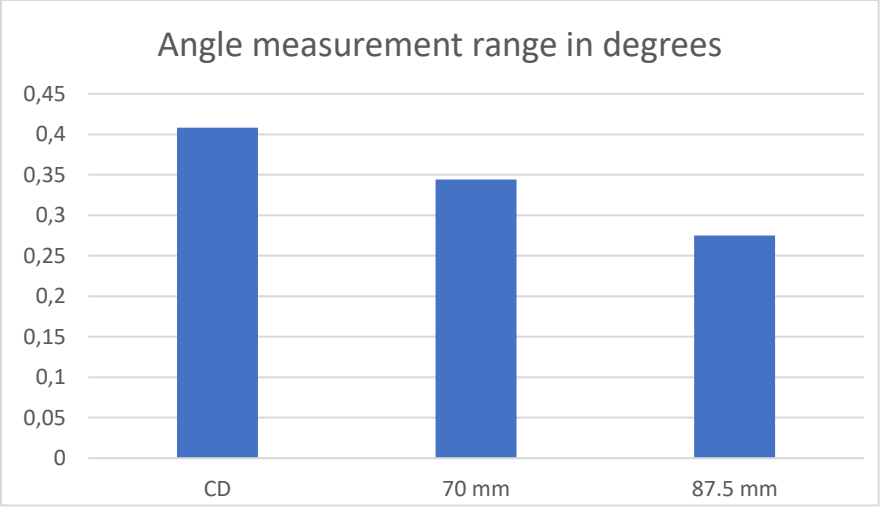

Figure 38: Angle measurement range of the attachment points from the current design (CD) and two combinations of symmetrically placed attachment points

Three symmetrically placed attachment points at a distance of 70 mm from the interface center yield better results than the attachment points of the current design. If the symmetrically placed attachment points are at a distance of 87.5 mm from the interface center, the angle measurement range is almost halved.

4.2.6 Contact pressure simulation comparison with the current design

The test model used in the RD&T analysis, see section 4.2.3, was analyzed in Ansys to ease comparison of the results. The simulation was performed in the same fashion as the simulations in 4.2.1. To hinder the unused holes from affecting the results, these were deactivated for each run. A model, with the attachment points of the current design was also tested in a similar fashion. Figure 39 shows the share of nodes with a pressure exceeding 0.2 MPa for each of the tested models. For pressure limits 0 MPa and 0.4 MPa, see Appendix *E: Contact pressure simulation tests with three contacts points and current design*.

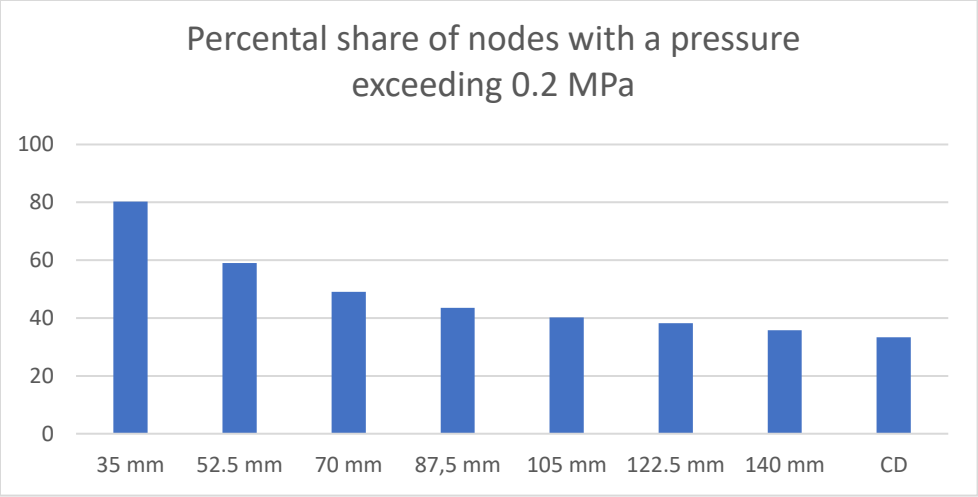

Figure 39: Percental share of nodes exceeding 0.2 MPa

The result show that, symmetrically placed attachment points has a positive effect on the pressure distribution.

4.3 Comparison of physical tests with simulation tests of current design

The result from the physical pressure test, see section 4.1.2, was compared to the simulation pressure test in order to verify the simulation. Figure 40 shows the imprint from a pressure test with a LLW Prescale film and the simulation pressure test result. Even though the simulation interface is simplified, a similar pattern is identified when comparing the two. High pressures are identified at the top and bottom of the interface.

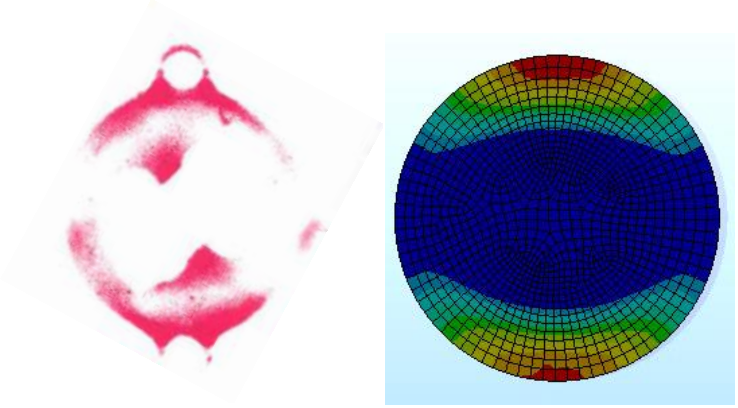

Figure 40: Pressure imprint from test with LLW film and simulation pressure test using positioning points from the current design

The effect of rigid body misalignment on the current design was most evident on the edges close to the vertical line of the interface where the measured angles were the largest, see Figure 37. This further indicates that the current attachment point placement gives lower pressures on the sides of the interface.

5 Concept Generation

The following chapter presents generated concepts for alternative radio mounting mechanisms. The concepts were generated with brainstorming. The ideas generated were roughly modelled in CAD to visualize the concepts and to make them easier to evaluate and compare.

5.1 Radio mounting concepts

For all solutions below, all interfaces connected to the coupler will remain the same as on the current design. This means that the component used to attach the radio to the coupler is secured with screws and it will be referred to as the *attachment frame* in all concept descriptions. This also means that the transition hub and coupler interface will be untouched. The attachment points between the radio and attachment frame will be positioned symmetrically around the waveguide interface on all concepts, based on the results of the simulations and physical tests, summarized in section 4.3.

Spring loaded screws

The coupler is equipped with a stiff plate, the attachment frame, with threaded holes that allows the radio to be mounted with screws, see Figure 41. The screws are mounted together with springs in order to get an even build-up of pressure. The solution can either have three or four screws.

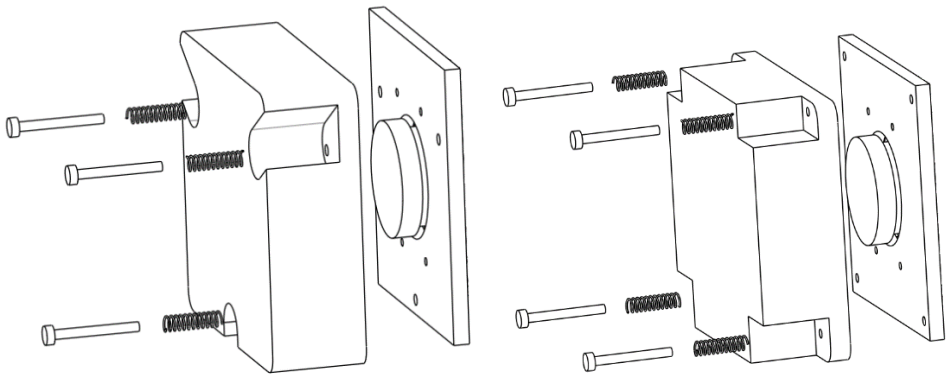

Figure 41: Spring loaded screws concepts with three and four screws respectively.

Deforming Plate

Similar to the existing design, the radio is mounted on hooks on a plate, attachment frame, and secured with a screw. By tightening the screw, the plate deforms until it meets the mating surface and thereby generating a buildup of pressure on the interface. What differentiates this design from the existing design is that the placement of the attachment points is symmetrical, see Figure 42.

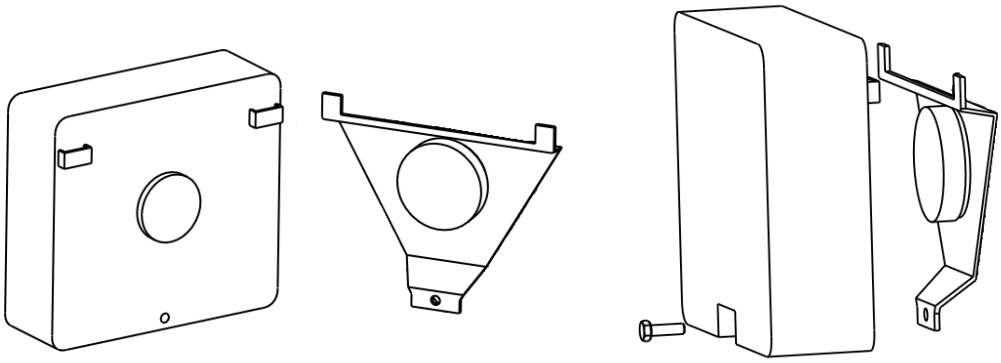

Figure 42: Deforming plate concept with one screw.

An alternative to this design is to have four attachment points instead of three, two hooks and two screws, see Figure 43.

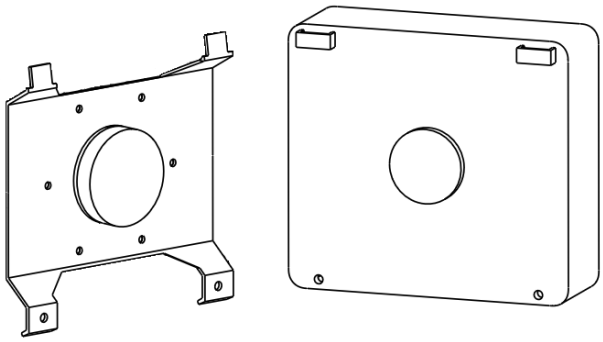

Figure 43: Deforming plate concept with two screws.

Cam lock

This solution utilizes a so-called cam lock coupling design. The radio is equipped with three levers that are symmetrically placed around the interface, see Figure 44.

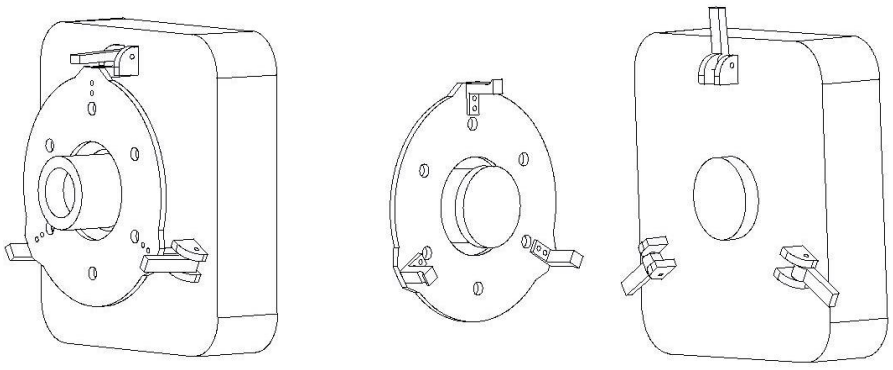

Figure 44: Camlock concept.

These levers are fitted into brackets on the radio and secured with pins. The attachment frame is designed with three grooves, the radio is secured the attachment frame by folding the levers on the radio, which in turn will clamp on the grooves. The radius around the axis of rotation of the lever increases as the levers are turned, meaning that more material is forced in between the groove and the axis of rotation and thus forcing the radio closer to the transition-hub. No tool is required on installation. Applying four levers to this solution would allow cross locking.

Wedges

The attachment frame is equipped with three wedges positioned in track grooves pointing towards the center of frame. The wedges are attached to screws that are used to adjust the position of the wedges. The radio interface has a conical shape that matches with the wedges. By placing the radio interface towards the transition hub interface and by tightening the wedge screws the radio is secured. The wedge screws convert the translation towards the center of interface into a horizontal translation of the radio interface, causing a buildup of contact pressure between the radio interface and the transition hub. This concept could also be designed with four wedges which allows cross locking.

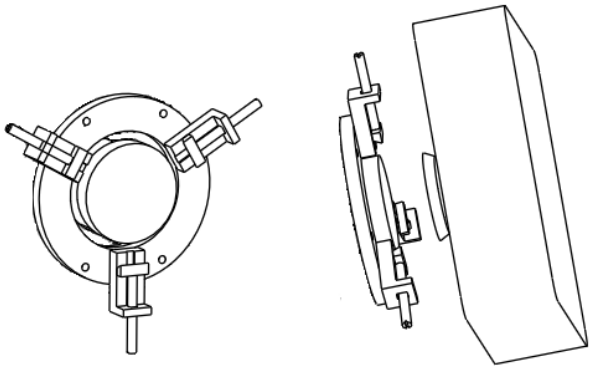

Figure 45: Wedges concept.

Screw Cap

The Screw Cap utilizes a so-called hygienic union often used in the food industry to connect pipes to each other. The interface on the radio side is encapsulated in an externally threaded male, attachment frame, see Figure 46. The male is then connected to the female using a loose internally threaded nut. As the nut is tightened it forces the radio towards the transition hub by applying pressure on a flange on the two, separately mounted, interface units. Since the nut needs an inner diameter greater than the diameter of the interface, the dimensions need to be fairly large, which requires the use of a spanner wrench to ease installation. The rigid body misalignment that occurs in the interface is in direct correlation with the tolerance in the thread.

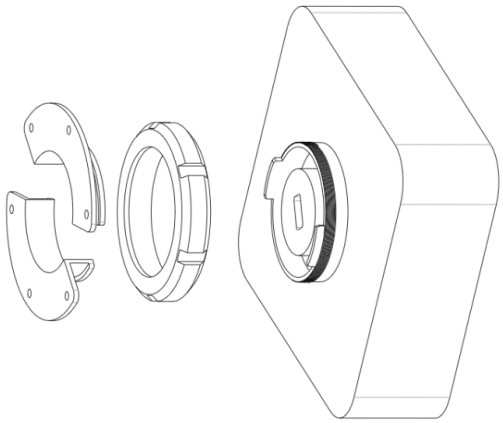

Figure 46: Screw cap concept.

Tri connector

The Tri connecter uses a clamp fitting locking configuration, see Figure 47. The attachment has a circular design and is secured to the reflector with screws. Both radio and attachment frame have circular flanges which are fixed together with a clamp, securing the radio.

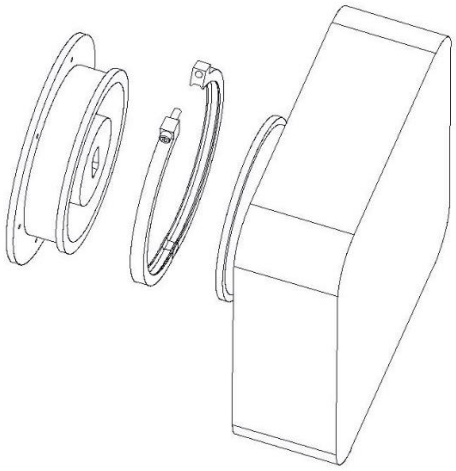

Figure 47: Tri connector concept.

Toggle Latches

The radio is equipped with three toggle latches, that are symmetrically placed around the interface, see Figure 48. These are during assembly connected to an attachment frame mounted directly on the reflector. If four toggle latches were to be used, cross locking would be possible, since the installer can lock two opposite latches at the time. The latches can be tightened by hand, meaning that no tools are required during installation of the radio.

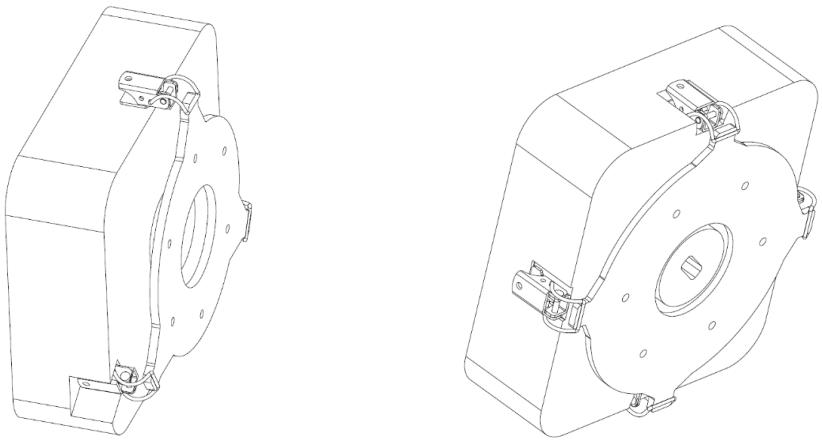

Figure 48: Toggle latch concepts with three and four latches respectively.

CPU

The solution has a mounting mechanism similar to that of a CPU in a desktop computer, see Figure 49. A metal latch is attached on each side of the radio and as they are folded down, they push down on the lips of plate placed on the radio. As the plate frame is pushed down, it in turn forces the radio to move towards the transition hub. When the latches reach their final position, parallel to the interface, they are connected to hooks to secure their position and ensure a constant pressure in the interface. The solution does not require any tools and both latches can be folded down at the same time.

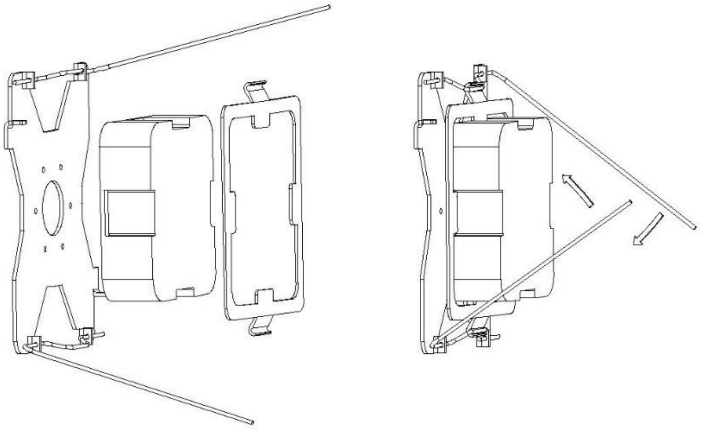

Figure 49: CPU concept.

6 Concept Evaluation and Elimination

The following chapter describes how the generated concepts were evaluated and how the concept elimination process was executed. Concept scoring was based on four criteria, time of in-house and at-site assembly process, and manufacturing and component cost.

6.1 DFA analysis in AviX

AviX is commonly used to identify areas of improvement on an existing product with regards the assembly process. In this case it has been used to compare the assembly process between several different product concepts. Two different DFA analyses were performed for each concept. The first analysis solely considered the manufacturing assembly process and focused on identifying the different assembly times. The current design is delivered with a pre-installed attachment frame (interface plate), therefore the first analysis considered the assembly of the attachment frame on the coupler as well as all associated components. The second analyses assessed the steps that the installer would perform on site, which is the mounting of the transition hub and radio.

Due to the simplicity of the concepts at this stage of the project a simplified DFA, *DFA2 Product level (Simplified)*, was performed in both analyses. Each component was scored based on five pre-defined categories in AviX; *Reachability*, considers restrictions during assembly; *Insertion*, considers how the design helps with insertion (e.g. guiding pins, chamfers etc.); *Holding Assembled Parts*, considers position stability of component after assembly; *Fastening Method*, considers required fastening methods; and *Separate Operations,* considers required operations after assembly. The score in each category was determined by three default criteria in AviX, resulting in a score of either 1, 3 or 9. This generated a total score for each concept and an estimated assembly time. Figure 50 shows and example of the process explained above. *Agg time* is the estimated assembly time.

DFX | DFA2 part level (MA) | DFA2 product level

Component	N.	G..	Reachability	Insertion	T..	Holdin...parts	Fasten...ethod	Separa...tions	DFA Score					
									Score	Score (%)	Agg Score	Agg Score (%)	Time	Agg Time
Camlock (3)									0		643	62 %		153,2
Camlock Hook 1 1 pcs	-	-	9	1	-	1	9	9	29	64 %			7,5	
CH Screw 1 1 pcs	-	-	9	1	-	9	3	3	25	56 %			6,5	
CH Screw 2 1 pcs	-	-	9	1	-	9	3	3	25	56 %			6,5	
Camlock Hook 2 1 pcs	-	-	9	1	-	1	9	9	29	64 %			7,5	
CH Screw 3 1 pcs	-	-	9	1	-	9	3	3	25	56 %			6,5	
CH Screw 4 1 pcs	-	-	9	1	-	9	3	3	25	56 %			6,5	
Camlock Hook 3 1 pcs	-	-	9	1	-	1	9	9	29	64 %			7,5	
CH Screw 5 1 pcs	-	-	9	1	-	9	3	3	25	56 %			6,5	
CH Screw 6 1 pcs	-	-	9	1	-	9	3	3	25	56 %			6,5	
Interface Plate 1 pcs	-	-	9	1	-	1	9	9	29	64 %			7,5	
Screw 1 1 pcs	-	-	9	1	-	9	3	3	25	56 %			6,5	
Screw 2 1 pcs	-	-	9	1	-	9	3	3	25	56 %			6,5	
Screw 3 1 pcs	-	-	9	3	-	9	3	9	33	73 %			6,2	
Screw 4 1 pcs	-	-	9	3	-	9	3	9	33	73 %			6,2	
Screw 5 1 pcs	-	-	9	3	-	9	3	9	33	73 %			6,2	
Screw 6 1 pcs	-	-	9	3	-	9	3	9	33	73 %			6,2	
Transition Hub 1 pcs	-	-	9	3	-	3	3	9	27	60 %			6,2	
Lever 1 1 pcs	-	-	9	3	-	1	9	9	31	69 %			7,2	
Pin 1 1 pcs	-	-	9	3	-	9	3	1	25	56 %			6,2	
Lever 2 1 pcs	-	-	9	3	-	1	9	9	31	69 %			7,2	
Pin 2 1 pcs	-	-	9	3	-	9	3	1	25	56 %			6,2	
Lever 3 1 pcs	-	-	9	3	-	1	9	9	31	69 %			7,2	
Pin 3 1 pcs	-	-	9	3	-	9	3	1	25	56 %			6,2	

Figure 50: Example of DFA analysis of the manufacturing assembly process of the Camlock 1 (3).

The DFA analysis results of the in-house and at site assembly process can be seen in Table 18 and Table 19.

Table 18: DFA analysis of In-house assembly process

In-house assembly process		
DFA2 Product level (Simpl.)	**Estimated Assembly Time (s)**	**Rank**
Camlock 1 (3 levers)	153,2	13
Camlock 2 (4 levers)	105,1	10
CPU	72,9	4
Deforming plate 1 (1 screw)	62,2	2
Deforming plate 2 (2 screws)	63,9	3
Screw Cap	85,1	5
Spring loaded Screws 1 (3 screws)	92,6	7
Spring loaded Screws 2 (4 screws)	92,8	8
Toggle latches 1 (3 latches)	107,3	11
Toggle latches 2 (4 latches)	113,9	12
Tri-Connector	56	1
Wedges 1 (3 wedges)	88,7	6
Wedges 2 (4 wedges)	101,1	9

Table 19: DFA analysis of at site assembly process

At site assembly process		
DFA2 Product level (Simpl.)	**Estimated Assembly Time (s)**	**Rank**
Camlock 1 (3 levers)	21,2	5
Camlock 2 (4 levers)	27,2	7
CPU	18,5	4
Deforming plate 1 (1 screw)	13,9	1
Deforming plate 2 (2 screws)	15,6	2
Screw Cap	16	3
Spring loaded Screws 1 (3 screws)	35,6	12
Spring loaded Screws 2 (4 screws)	28,3	9
Toggle latches 1 (3 latches)	30,5	10
Toggle latches 2 (4 latches)	27,5	8
Tri-Connector	24,5	6
Wedges 1 (3 wedges)	31,1	11
Wedges 2 (4 wedges)	37,3	13

6.2 Concept cost assessment

All concepts have been scored and ranked on cost. The score consists of two sub-scores, one that takes the manufacturing cost of components that are deemed not to be standard components into account, and one score that considers the cost of the standard components in each concept. The manufacturing cost score is strictly relative, meaning that the concepts cost is ranked and compared to each other. The standard component cost score is based on price data from mcmaster.com.

6.2.1 Manufacturing cost

In order to compare the different concepts manufacturing cost, data from *CES Edupack* was used. For each concept, the necessary manufacturing processes needed to produce the concepts components

were identified, see Table 20. Concepts that require a certain process for one of its components are marked with a *1* and concepts that require a certain process to manufacture two of its components are marked with a *2*, and so forth.

Table 20: Manufacturing cost matrix

	Casting	Drilling	Milling	Rod bending	Sheet metal bending	Stamping	Tapping	Turning
Camlock 1 (3 levers)	*3*	*4*	*1*				*1*	
Camlock 2 (4 levers)	*3*	*2*	*1*					
CPU	*1*	*1*	*3*	*1*	*2*			
Deforming plate (1 screw)	*1*	*2*	*2*			*1*	*2*	
Deforming plate (2 screws)	*1*	*2*	*2*			*1*	*2*	
Screw Cap	*2*	*2*						*1*
Spring loaded screws 1 (3 screws)	*1*	*2*	*2*				*2*	
Spring loaded screws 2 (4 screws)	*1*	*2*	*2*				*2*	
Toggle latches 1 (3 latches)	*1*	*2*	*1*				*1*	
Toggle latches 2 (4 latches)	*1*	*2*	*1*				*1*	
Tri Connector	*2*	*1*						*2*
Wedges 1 (3 wedges)	*3*	*2*	*1*				*1*	*1*
Wedges 2 (4 wedges)	*3*	*2*	*1*				*1*	*1*

CES Edupack was then used to identify the following parameters, *relative tooling cost*, *relative equipment cost* and *labor Intensity f*or each of the manufacturing processes. These parameters are by the software graded as *low*, *medium* or *high.* This grading was quantified into a scoring system, in which the processes would be given a score of one to three for each of the three parameters. The sum of these scores would give a *total process score* for a specific manufacturing process, where a low score represents a low process cost and a high score represents a high process cost, see Table 21.

Table 21: Process cost scores

	Relative tooling cost	Relative equipment cost	Labor intensity	Total process score
Casting	*2*	*2*	*2*	*6*
Drilling	*1*	*2*	*3*	*6*
Milling	*1*	*3*	*2*	*6*
Rod bending	*2*	*2*	*1*	*5*
Sheet metal bending	*3*	*3*	*2*	*8*
Stamping	*3*	*2*	*1*	*5*
Tapping	*2*	*3*	*2*	*7*
Turning	*2*	*3*	*2*	*7*

The total process score for each of the manufacturing methods is then multiplied with the number of times it is needed to produce a certain concept. The sum of these scores gives a *total manufacturing cost score* for each of the concept, see Table 22. A high value represents a relatively high manufacturing cost and a low value represents a relatively low manufacturing cost.

Table 22: Total manufacturing cost score

	Total manufacturing cost score		Manufacturing cost rank
Camlock 1 (3 levers)	*55*	**Screw Cap**	*1*
Camlock 2 (4 levers)	*36*	**Toggle latches 1 (3 latches)**	*1*
CPU	*51*	**Toggle latches 2 (4 latches)**	*2*
Deforming plate 1 (1 screw)	*49*	**Tri Connector**	*3*
Deforming plate 2 (2 screws)	*49*	**Camlock 2 (4 levers)**	*3*
Screw Cap	*31*	**Spring loaded screws 1 (3 screws)**	*4*
Spring loaded screws 1 (3 screws)	*44*	**Spring loaded screws 2 (4 screws)**	*5*
Spring loaded screws 2 (4 screws)	*44*	**Deforming plate 1 (1 screws)**	*6*
Toggle latches 1 (3 latches)	*31*	**Deforming plate 2 (2 screws)**	*7*
Toggle latches 2 (4 latches)	*31*	**Wedges 1 (3 wedges)**	*8*
Tri Connector	*32*	**Wedges 2 (4 wedges)**	*9*
Wedges 1 (3 wedges)	*50*	**CPU**	*10*
Wedges 2 (4 wedges)	*50*	**Camlock 1 (3 levers)**	*11*

Concepts with the same score have been given the same rank, except for concepts of the same type, for which the concepts with a lower number of fastening elements have been given a higher rank. For example, *Toggle latches 1 (3)* and *Toggle latches 2 (4)* have the same total manufacturing cost score but *Toggle latches 1 (3)* is given a higher rank since it has fewer fastening elements.

6.2.2 Standard part cost

Parts that are considered to be standard components are not included in the manufacturing cost score, and therefore do not affect the result in said score. The following table shows the excluded parts for each concept, see Table 23.

Table 23: Excluded standard part for all generated concepts.

	Excluded parts
Camlock 1 (3 levers)	*Attachment Frame Screws (6), Attachment Frame Spacers (6), Pins (3)*
Camlock 2 (4 levers)	*Attachment Frame Screws (6), Attachment Frame Spacers (6), Pins (4)*
CPU	*Attachment Frame Screws (6), Attachment Frame Spacers (6)*
Deforming plate 1 (1 screw)	*Attachment Frame Screws (6), Attachment Frame Spacers (6), Lock screw (1)*
Deforming plate (2 screws)	*Attachment Frame Screws (6), Attachment Frame Spacers (6), Lock screws (2)*
Screw Cap	*Attachment Frame Screws (6), Attachment Frame Spacers (6), Lock nut (1)*
Spring loaded screws 1 (3 screws)	*Attachment Frame Screws (6), Attachment Frame Spacers (6), Lock screws (3), Springs (3)*
Spring loaded screws 2 (4 screws)	*Attachment Frame Screws (6), Attachment Frame Spacers (6), Lock screws (4), Springs (4)*
Toggle latches 1 (3 latches)	*Attachment Frame Screws (6), Attachment Frame Spacers (6), Toggle latch screws (6), Toggle latches (3)*
Toggle latches 2 (4 latches)	*Attachment Frame Screws (6), Attachment Frame Spacers (6), Toggle latch screws (8), Toggle latches (4)*
Tri Connector	*Attachment Frame Screws (6), Attachment Frame Spacers (6), Tri Connector (1)*
Wedges 1 (3 wedges)	*Attachment Frame Screws (6), Attachment Frame Spacers (6), Wedge screw (3)*
Wedges 2 (4 wedges)	*Attachment Frame Screws (6), Attachment Frame Spacers (6), Wedge screw (4)*

The standard component cost is calculated for each concept. To get a fair comparison, all component costs are gathered from the same source, *mcmaster.com*, and shared parts are excluded. The accumulated standard component cost for each concept rounded to closest tens. The results can be seen in Table 24.

Table 24: Standard part cost score for all generated concepts

	Non-Shared parts	Total cost (USD)	Rounded cost (USD)	Component cost score
Camlock 1 (3 levers)	*Pins (3)*	0,1473	*0*	*0*
Camlock 2 (4 levers)	*Pins (4)*	0,1964	*0*	*0*
CPU			*0*	*0*
Deforming plate 1 (1 screw)	*Lock screw (1)*	0,1798	*0*	*0*
Deforming plate 2 (2 screws)	*Lock screws (2)*	0,3596	*0*	*0*
Screw Cap	*Lock nut (1)*	62,67	*60*	*6*
Spring loaded screws 1 (3 screws)	*Lock screws (3), Springs (3)*	6,7554	*10*	*1*
Spring loaded screws 2 (4 screws)	*Lock screws (4), Springs (4)*	9,0072	*10*	*1*
Toggle latches 1 (3 latches)	*Toggle latch screws (6), Toggle latches (3)*	11,8836	*10*	*1*
Toggle latches 2 (4 latches)	*Toggle latch screws (6), Toggle latches (3)*	15,8448	*20*	*2*
Tri Connector	*Tri Connector (1)*	70,25	*70*	*7*
Wedges 1(3 wedges)	*Wedge screw (3)*	2,211	*0*	*0*
Wedges 2(4 wedges)	*Wedge screw (4)*	2,948	*0*	*0*

6.3 Concept elimination

An elimination matrix was made based on the data from the DFA analysis and the cost assessment. The data was divided into four categories, *In-house assembly process*, *At site assembly process*, *Manufacturing cost*, and *Component cost*. The data from each category was translated into a score between 0 to 20. Each category was also given a weight based on importance that was multiplied by the translated score. Since the relation between the component cost and the manufacturing cost is unknown, a total of four different weight cases was tested. Each concept was also evaluated based on the requirements, resulting in direct elimination of some concepts.

6.3.1 Concept elimination result

The result can be found in Appendix *F: Concept elimination matrices*. Deforming plate 1 and 2 and the CPU got the highest scores in all four evaluations and the other concepts were eliminated. The three remaining concepts will be further analyzed in the following section, see section 6.4

6.4 Concept design analysis

The three remaining concepts are discussed and evaluated based on the criteria in the concept elimination as well as design factors that could affect performance.

CPU

The main benefit of the CPU is that it offers simple assembly without the need for tools. The idea behind the concept is that a metal plate translates two forces, generated by the latches, into four contact forces on the radio, creating an even pressure distribution on the waveguide interface. However, this type of force distribution will result in a convex deformation of the plate and uneven force distribution on the four contact points of the radio. This could be solved by applying varying thickness to the plate, although it will increase the complexity of the plate and increase manufacturing costs. Even though in theory, even force distribution on the four contact points is possible, it would be difficult to achieve, and the concept is therefore eliminated.

Deforming plate 1 & Deforming plate 2

The main design benefit with *Deforming plate 1* is that it can be secured with one screw operation. This is beneficial as it shortens assembly time and it lowers the number of loose components compared to the other two concepts. As the screw is tightened, the hooks of the attachment frame and the material around the screw on the attachment frame starts deforming, meaning that the frame acts as a spring and the force caused by it is therefore dependent on how much it deforms. *Deforming plate 2* works in the same fashion as *Deforming plate 1* but adds one more screw on the bottom of the attachment plate. The relation between rigid body misalignment and deformation, see section 4.2, is not known but rigid body misalignment is believed to be more impactful since the radio is fairly stiff. Since the radio has a quadratic shape, *Deforming plate 2* makes it possible to utilize the backside of the radio to a fuller extent, meaning that the attachment points can be placed further from the center of interface which is known to reduce rigid body misalignment, see Figure 51. Therefore, *Deforming plate 1* is eliminated and *Deforming plate 2* will be further developed and investigated.

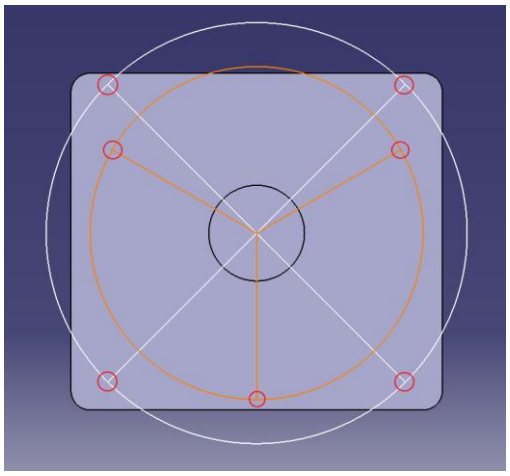

Figure 51: Difference in distance to interface between three (orange colored) and four attachment points (white colored).

6.4.1 Pressure distribution simulation comparison of Deforming plate 2 and current design

The approximate positioning of the attachment points of *Deforming plate 2*, see Figure 52, were compared to the positioning points from the current Ericsson design by performing a pressure simulation in the same way as in the simulations in Section 4.2.1.

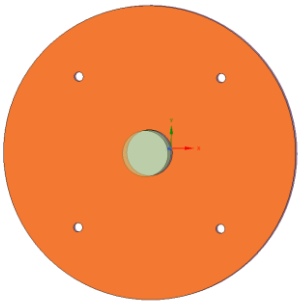

Figure 52: Simulation model with attachment points prototype design

The distribution of pressure is more even in the prototype design compared to the current design, see Figure 53.

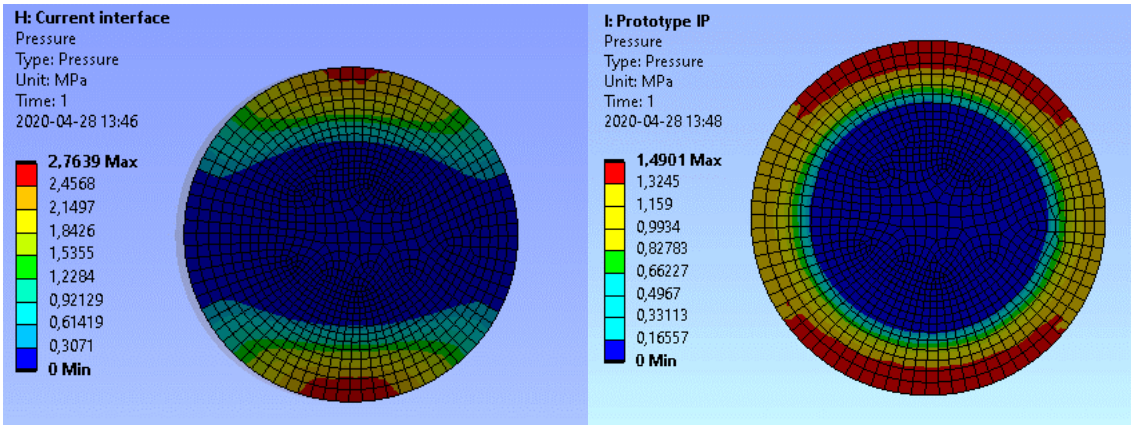

Figure 53: Interface pressure distribution with current and Deforming plate 2 attachment points

The area which is affected by a pressure above 0,2 MPa equals 33 % of the contact area using the contact point positioning from the current design. Performing the same analysis using the contact point positioning from the prototype yields a result of 38%. The conclusion is that the *Deforming plate 2* interface could give a more even pressure distribution than that of the current design.

7 Prototype

The following chapter describes the process of developing and testing a physical prototype of the concept *Deforming plate 2*. The overall design of the protype and its purpose are presented and all subassemblies of the prototype, and their respective design processes, are described in detail. Lastly, the testing procedure and results are presented and detailed, and a comparison with the testing results of the current design is made.

7.1 Overall prototype design

The prototype consists of two components, the *Attachment frame* and the *Radio*. These are assembled together with current reflector, coupler and transition hub, see Figure 54.

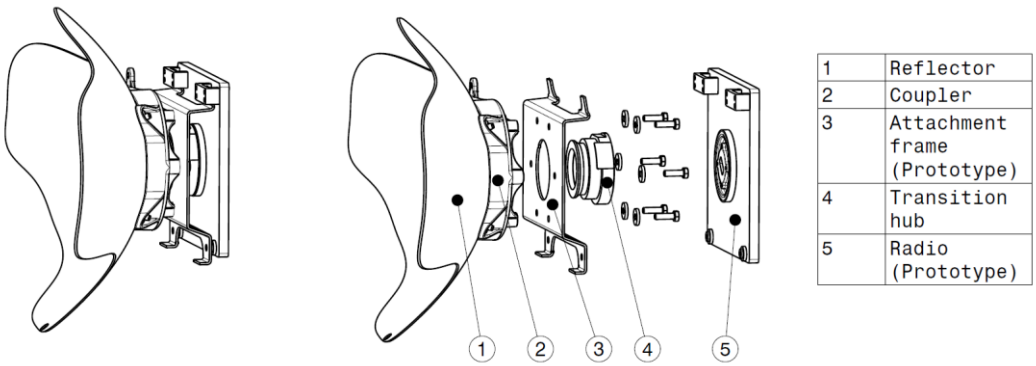

Figure 54: Prototype assembly

The attachment frame is designed to be able to mount on the existing coupler, using six mounting screws and washers. The dimensions and placement of the holes for the transition hub and mounting screws on the attachment frame are the same as the one the interface plate of the current design in order to keep compatibility with the coupler. After the attachment frame has been assembled on to the coupler, the radio is hung on the hooks of the attachment frame and the two screws are tightened. As they are tightened, the hooks and the material around the screw holes start deforming which causes a reaction force that acts on the hooks and around the screw holes of the radio. After the screws are fully tightened, meaning that the part of the attachment frame around the mounting screws has come in contact with the radio, the reaction forces caused by the attachment frame deformation, $F_{1.AF}$, $F_{2.AF}$, $F_{3.AF}$, and $F_{4.AF}$, generates reaction forces on the attachment points on the radio, $F_{1.R}$, $F_{2.R}$, $F_{3.R}$, and $F_{4.R}$, which in turn generates a reaction force on the interface, $F_{Interface}$, see Figure 55.

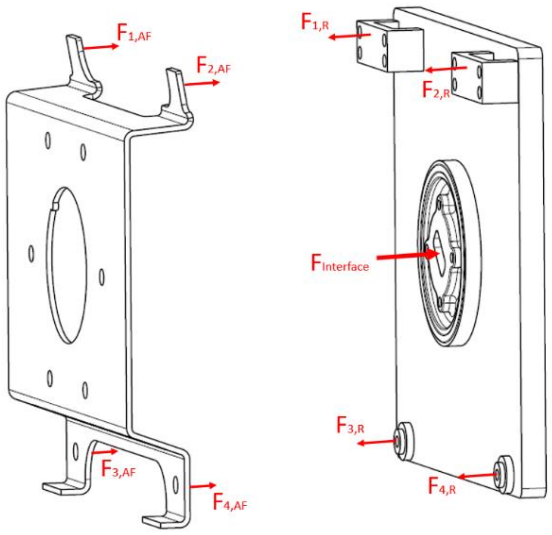

Figure 55: Force distribution on attachment frame and radio

Since the deformation around the screw holes is hindered by the meeting surfaces of the radio, a similar deformation and reaction force is created each time the radio is mounted.

The purpose of the prototype is to test how the changed mounting design affects pressure and pressure distribution in the interface and how the new design compares to the current one. This will be done by using a microcapsule film. In order to allow for a just comparison of the microcapsule pressure film test, the actual interface and the transition hub are identical to that of the current design, meaning that the only design parameter that affects the result is the mounting design.

7.1.1 Attachment frame design process

The initial design approach of the attachment frame was to design the cross-section of the plate to resemble the current design. The objective when designing the prototype was to make the contact points of the attachment frame deform to such an extent, that reaction forces applied on the radio would create a force in the waveguide surface of the interface that fulfilled the force requirements. Ideally, this force would be evenly distributed on the contact points, in order to create an even pressure.

Measurement *A* is the allowed deformation in the screw hole attachment points and measurement *B* is the allowed deformation in the hook attachment points used in the first design iteration, see Figure 56. These together with the angles of the plate bends were parameters that could be changed the in analysis.

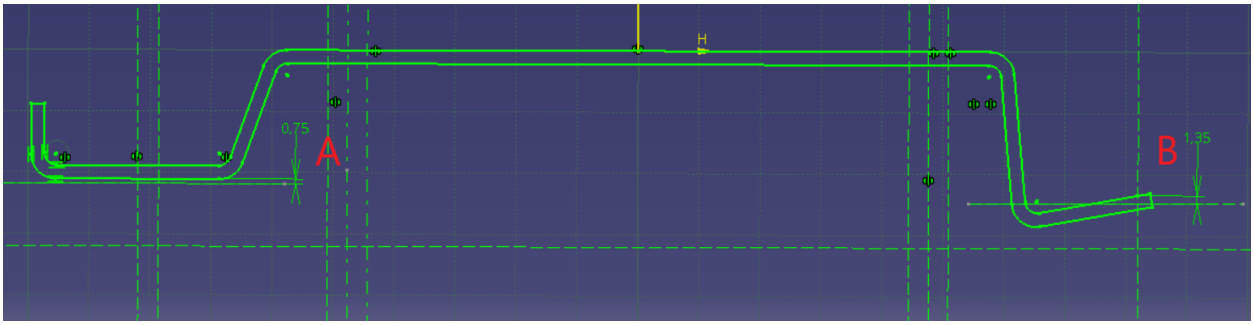

Figure 56: Attachment frame cross-section

Ansys was used to test the force balance in the attachment frame design. The force requirement in the waveguide surface of the interface is 1400 ± 600 N. The O-ring absorbs roughly 300 N and the resulting force sum used for analysis was therefore 1700 N (1400 N + 300 N). Each attachment point was assigned with 425 N to simulate even force distribution. The forces were assumed to be perpendicular to the base of the attachment frame, see Figure 57.

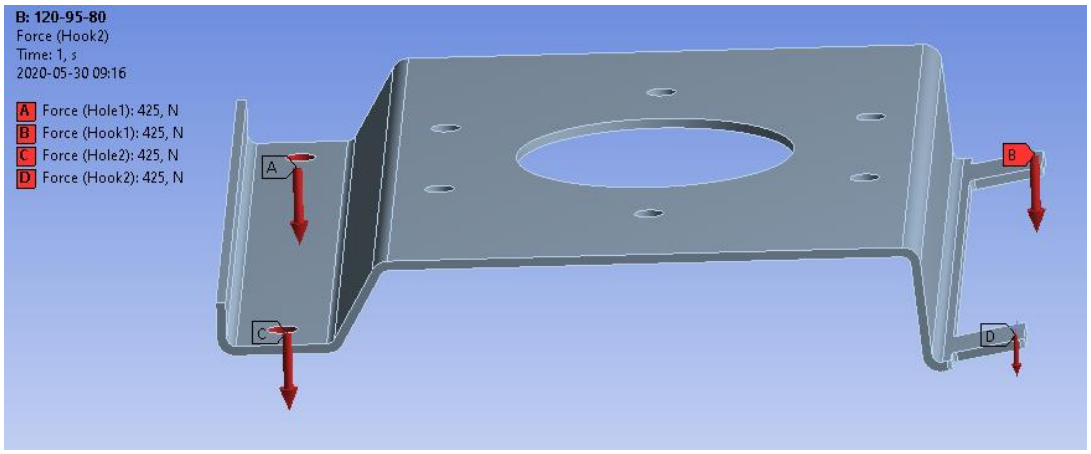

Figure 57: Attachment frame with applied forces

The screw holes, used to fix the attachment frame to the coupler, were assigned clamp constraints to secure the attachment frame. Deformation probes were used to register the deformation in Z-direction in the attachment points. The goal was to create a design where the deformation was relatively even in each attachment point. The material used in the analysis was structural steel with a Youngs modulus of 205 MPa. The design parameters were the bending angles of the plate, corner radius, and the allowed deformation on the attachment points. The design process was iterative and had three steps, simulating deformation, analyzing the results, and changing the geometry based on the results.

Ideally, a large elastic deformation is preferable since the force generated by the deformation is less sensitive to tolerances. The bottom part of the plate was initially stiff. A relatively small deformation caused a reaction force equal to 425 N, which is problematic since a small deformation would require

tight tolerances. To reduce stiffness, multiple small holes and a pocket were added, see Figure 58.

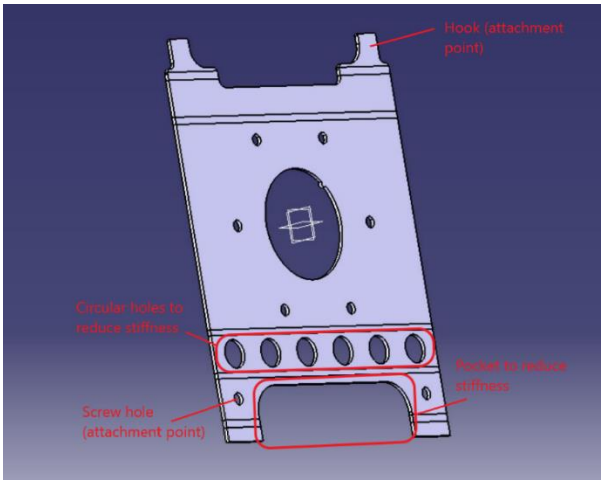

Figure 58: Attachment frame design in unfolded view

The corners of the hooks experienced high stress concentrations, around 500 MPa. The initial model had infinitely sharp edges in the area that suffered from these stress concentrations. Which is known to cause high stresses. Rounds were therefore added. The result was that the stress reduced to 460 MPa, see Figure 59.

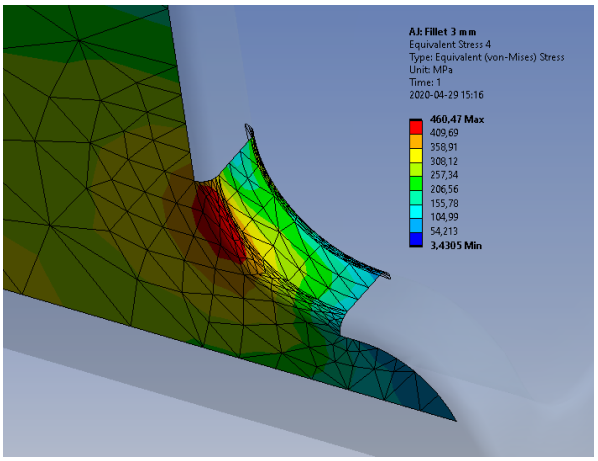

Figure 59: Hook stress concentration

The edge of the circular holes experienced high stress concentrations, 435 MPa, see Figure 60. This was however considered acceptable since the hooks experienced higher levels of stress. The choice was therefore to use a steel with a yield strength of 500 MPa for the prototype.

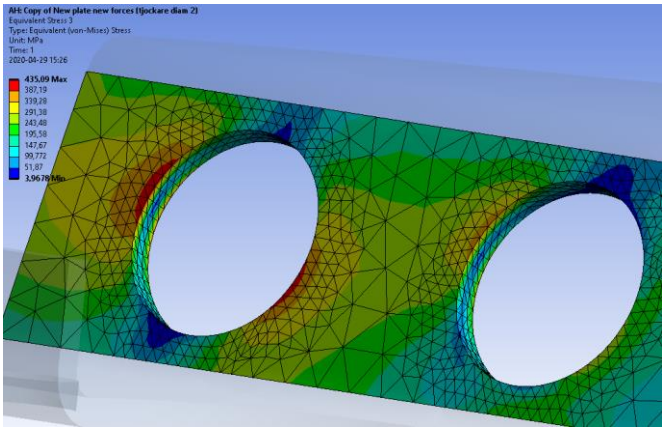

Figure 60: Hole stress concentration

The final design of the plate had an allowed deformation of 1,2 mm (screw holes) and 1,3 mm (hooks). The final plate design can be seen in Figure 61.

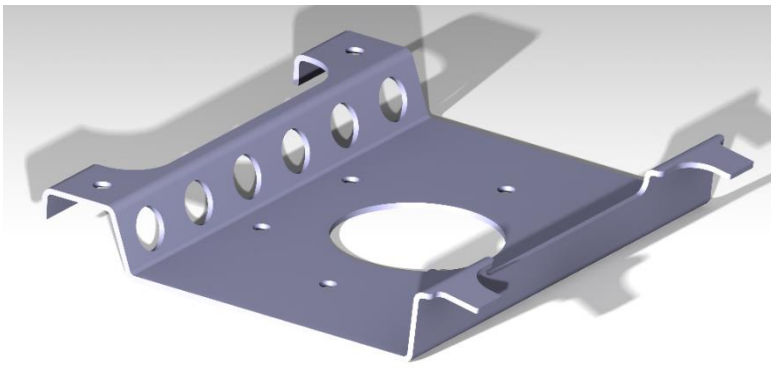

Figure 61: Render of the final attachment frame in folded view

7.1.2 Radio design process

Since the attachment frame does not fit the current radio, due to the changed attachment points, a simplified version of the radio was designed for the prototype. The radio interface was designed to be similar to the current radio interface design in order to get comparable results in the film tests. All attachment points on the radio prototype were designed in order to match with the deformation of the attachment frame. In order to be able to control where the contact between the radio and the attachment frame hooks occur, a small chamfer was added on the opposing loops of the radio, see Figure 62.

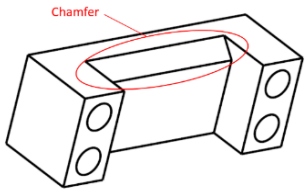

Figure 62: Radio loop chamfer

The chamfer creates a line-contact between the loops of the radio and the hooks of the attachment frame. Figure 63 shows a cross-section of the radio loop and attachment frame hook, and the required deformation, *B*, of the hook.

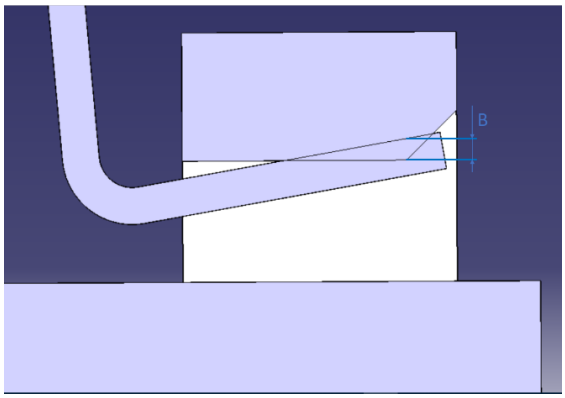

Figure 63: Required distance of hook deformation, B

The design was tested in Ansys to analyze deformation and stress. The waveguide interface was clamped and the attachment points, hocks and screw holes, where assigned 425 N in each, giving a force sum of 1700 N, see Figure 64. Deformation probes were put on the attachment points to measure deformation. The material used was structural steel with a Youngs modulus of 200 GPa.

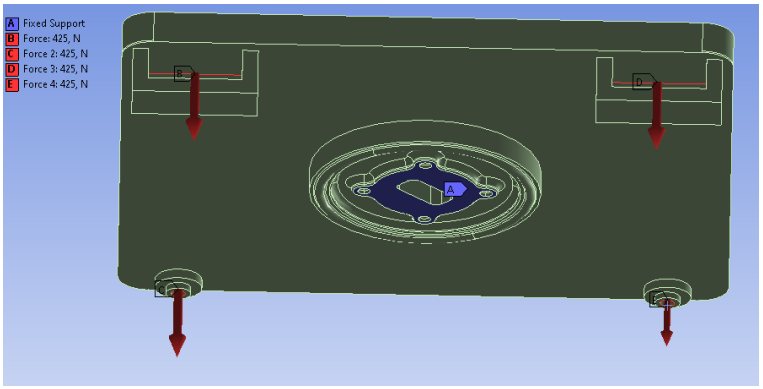

Figure 64: Radio prototype constraints

The goal was to make the deformation in the attachment frame generate most of the force. Therefore, the radio was designed to be as stiff as possible. The deformation in the attachment points where 0,05 mm. This is an acceptable deformation as it is less than 5 % of the deformation in the attachment points

on the attachment frame. The highest stress level was around 47 MPa, the material chosen for the radio was therefore 355 steel with a yield strength of 355 MPa, which was the standard steel used by the prototype supplier.

7.2 Prototype testing using Fujifilm Prescale

Contact pressure tests were performed using Fujifilm Prescale, similar to the test performed on the current design, see section 6.1.2. The components used in the test were the current reflector, coupler and transition hub, and the prototype attachment frame and radio, see Figure 65 and Figure 66.

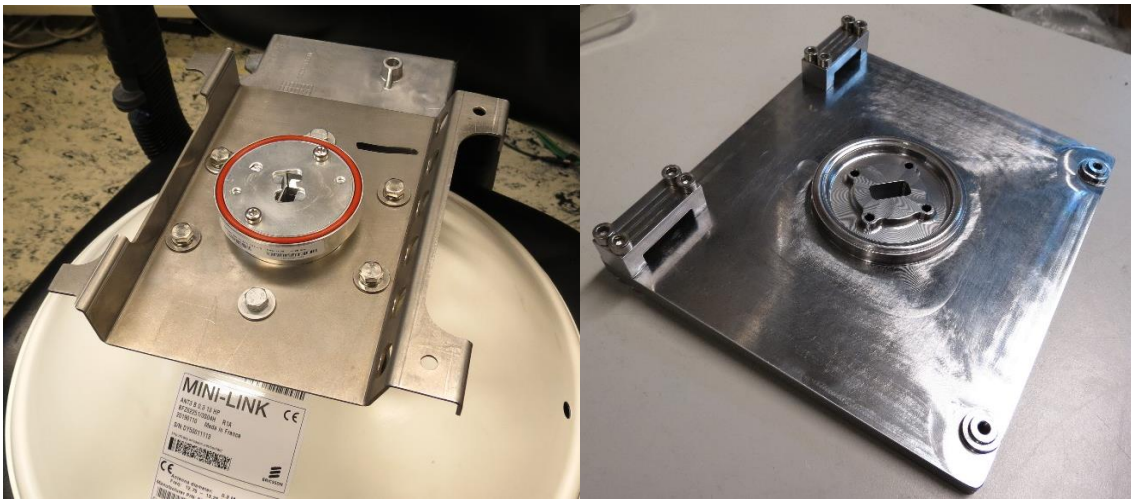

Figure 65: Attachment frame and radio prototype

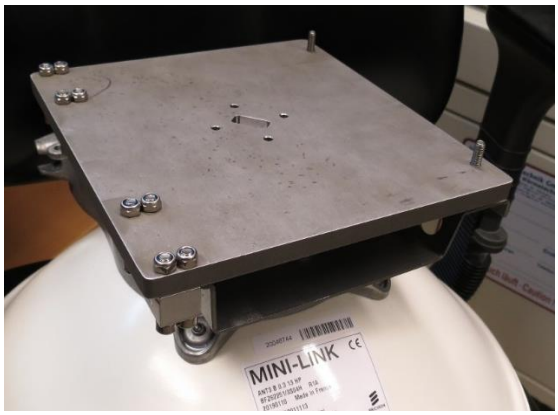

Figure 66: Prototype assembly

The film used to test contact was LLLW, since it was the film that most clearly showed pressure distribution in the testing of the current design, see Appendix *C: Fuji Film contact test*. Three attachment frames where manufactured and all were tested twice to increase the reliability of the results.

7.2.1 Prototype film test results

Results from the prototype film tests can be seen in Appendix *G: Contact pressure test of prototype with Fujifilm Prescale (LLLW)*. The overall results of the film tests show that there is almost total area coverage of pressure in the waveguide interface, see Figure 61.

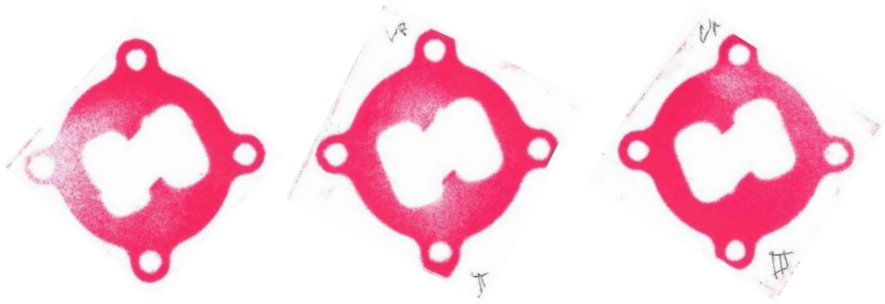

Figure 61: Pressure coverage of attachment frame 1,2, and 3.

The first test with attachment frame 1 shows zero pressure coverage in the upper right corner of the interface, see Figure 62. Attachment frame one has a defect, where the angles of the hooks slightly differs from each other. In theory, this should create an uneven force distribution between the attachment points and is likely the cause of lower pressure coverage.

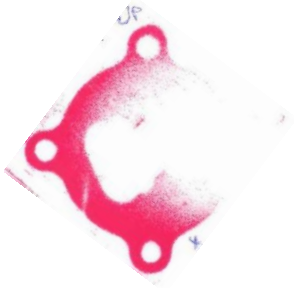

Figure 62: Pressure coverage on attachment frame 1.

The pressure imprint in the prototype tests has a larger area compared to that of the current design (using LLLW film), see section 6.1.2. However, the color density on the imprints in the prototype tests indicates that the pressure limit of the film is exceeded, which suggests that the prototype waveguide interface is subject to a higher contact pressures than the current waveguide interface.

8 Discussion

In the following chapter, a general discussion regarding the results of the project and the used methodology is given. Suggested further development steps are detailed and presented.

8.1 Overall product development methodology

The project required a large information gathering phase in its early stages, both in order to understand the underlying technology and the product structure, and to identify potential areas of improvement. Uneven pressure distribution in the waveguide surface was believed to be one of the underlying reasons for RF leakage and in order to investigate if this hypothesis was correct, three different approaches were used. The accuracy of the methods varies. The pressure film tests does not take manufacturing variation into account since only one radio was used when performing the tests. In order to perform the contact analysis in Ansys, simplifications and assumptions were made, e.g. the overall geometry of the models used. In the rigid body misalignment analysis, the test part representing the radio was a rigid body, which is not actually the case since the radio deforms during assembly. However, despite the simplifications, the result from all three approaches points in the same direction, meaning that the pressure on the sides of the waveguide surface is lower compared to the top and bottom, due to the attachment points placement of the current design. The choice to use several approaches also meant that this part of the project took a substantial part of the available time.

The main takeaway from the problem analyses was that the contact point placement in relation to the interface affects the distribution of pressure in the waveguide surface, and that a symmetrical placement of the attachment points would generate better results. In order to analyze a concept on pressure distribution, a certain stage of development needs to have been reached, where the overall geometry is set and materials are selected. When the concept elimination was made, this stage had not been reached and the elimination had to be based on other criteria. The criteria that laid the foundation of the selection was cost and assemblability. Ideally, concept elimination would also have been based on some type of pressure distribution analysis.

In the cost ranking, based on data gathered from CES Edupack, rough assumptions where made, but was deemed necessary in order to perform an objective comparison.

The result of the Fujifilm Prescale tests on the prototype was that the pressure coverage on the waveguide interface was improved compared to the current design. However, the results indicate the pressure limit of the film is likely exceeded. This is problematic as it could mean that the force requirement of the waveguide interface is violated. To get reliable results, the force should have been tested as well. The waveguide interface of prototype has a different surface roughness than the current design which is likely to have had an effect on the results.

8.2 Methodology for selecting testing methods

The purpose of investigating different test methods for leakage, surface contact and force was to identify methods that could improve testing and give objective results. No specific performance requirement regarding measurement error is given in the report since the purpose was to investigate potential test methods rather than identify one ideal method. However, data regarding performance and cost was identified to ease comparison for future testing method selection.

8.3 Further development

The prototype purpose was to test how the attachment frame affects the pressure distribution in the waveguide interface, in order to identify what effect the changed placements and number attachment points has. To go from prototype to product, the following aspects have been identified as recommended steps for further development.

Since the results of the prototype tests showed that the force requirement might be violated, the recommendation is to test the force by choosing one of the suggested force testing methods. The new updated design is believed to improve pressure distribution over the waveguide surface, the same is thought to happen in the O-ring, this however has to be tested. The prototype was manufactured based on the nominal design. Tolerances needs to be set based on a thorough tolerance analysis that studies the effect that the tolerances have on the forces in the attachment frame and the pressure distribution on the waveguide surface. Another aspect that needs to be considered is the usability of the design. The fastening method compared to current design is not changed but the number of fastening elements is increased, meaning that assembly will be slightly increased. How large this increase in assembly time is and the affect it has needs to be studied. The attachment plate in the prototype is made of a structural steel with a yield strength of 500 MPa, but more aspects other than the yield strength needs to be considered, e.g. corrosion resistance and surface treatment. The prototype was not intended to test the waveguide port alignment. Due to time constraints, port alignment has not been investigated, but this is an aspect that could potentially be improved. The shape and the surface roughness of waveguide interface could also be further analyzed.

If a setup using load cells is chosen, the test rig has to be designed and the way it affects the results has to be analyzed.

9 Conclusion

The main purpose of the project was to improve the current radio design regarding RF- and water leakage and suggest potential methods for testing the product in regard to said leakage types.

By simulations of pressure distribution, analysis of rigid body misalignment and physical tests using pressure sensitive films, it was found that the placement of the attachment points on the current design could cause uneven pressure distribution in the waveguide interface. The simulations also showed that a symmetrical attachment point placement improves the pressure distribution.

A new and redesigned model with four attachment points, symmetrically placed around the interface was developed and tested with a prototype. The test utilized the same type off pressure sensitive film that was used to test the current design and the results shows the pressure film imprints with the prototype have a larger coverage area. However, since the imprints have a very high color density compared to that of the current design, the force acting on the waveguide surface is potentially exceeding the upper limit of the force requirement.

No actual analysis regarding water leakage was performed but a more even pressure distribution in the waveguide interface is believed to create a more even pressure distribution on the O-ring as well, and thereby creating a better seal.

Four different methods for testing water leakage have been identified. Of these, mass flow sensing, is deemed to be the most suitable for the radio assembly, since it can detect leakage rates smaller than the maximum allowed leakage rate, is the least costly of the investigated methods and can test products of different internal volume without the need for recalibration.

Three alternative setups, A, B and C have been suggested for testing force and contact in the interface. Setup A includes a piezoresistive pressure senor system that can measure both force and contact simultaneously. Setup B includes a microcapsule film intended for contact measurement and a load cell-based rig for force testing. Setup C includes a microcapsule film intended for contact measurement and force sensing resistors for force measurement.

10 References

[1] S. Faruque, "Introduction to Radio Frequency," in *Radio Frequency Propagation Made Easy*, Springer, Cham, 2015.

[2] M. Lee, "Polarization," in *Optics for Materials Scientists*, Apple Academic Press , 2019.

[3] K. Fujimoto, "Antenna Polarization," in *Mobile Antenna Systems Handbook*, Artech House, 2008.

[4] P. Angueira and J. Romo, "INTRODUCTION TO MICROWAVE LOS LINK SYSTEMS," in *Microwave Line of Sight Link Engineering*, John Wiley & Sons, Incorporated, 2012.

[5] X. C. Tong, "Hollow Waveguides," in *Advanced Materials for Integrated Optical Waveguides*, Springer, Cham, 2014.

[6] T. Itoh, "Waveguides and Resonators," in *Reference Data for Engineers (Ninth Edition)*, Newnes, 2002.

[7] A. F. Harvey, "STANDARD WAVEGUIDES AND COUPLINGS FOR MICROWAVE EQUIPMENT," *Proceedings of the IEE - Part B: Radio and Electronic Engineering,* 1955.

[8] D. H. Evans, "Statistical Tolerancing: The State of the Art," *Journal of Quality Technology,* pp. 188-195, 1974.

[9] R. Söderberg, L. Lindkvist and C. Wickman, "Improving decision making by simulating and visualizing geometrical variation in non-rigid assemblies," *CIRP Annals,* pp. 175-178, 2008.

[10] A. Dagman, R. Söderberg and S. Hoffenson, "Tolerance Specification Optimization for Economic and Ecological Sustainability," 2013.

[11] P. D. Rufe, Fundamentals of Manufacturing, Society of Manufacturing Engineers, 2013.

[12] RD&T, "RD&T Tool," [Online]. Available: http://rdnt.se/tool.html. [Accessed 01 06 2020].

[13] R. Söderberg, *Wingquist Laboratory for Digital Product Realization,* 2018.

[14] G. Boothroyd, P. Dewhurst and W. A. Knight, Product design for Manufacture and Assembly, CRC Press, 2010.

[15] G. Boothroyd and P. Dewhurst, DESIGN FOR ASSEMBLY, Penton/IPC, Inc, 1984.

[16] J. Moultrie and A. M. Maier, "A simpliefied approach to design for assembly," *Journal of Engineering Design,* 2014.

[17] Avix, "Design for Assembly - an Avix Suite Module," [Online]. Available: https://www.avix.eu/process-mapping-tools/avix-dfx. [Accessed 01 06 2020].

[18] O. Ljung, *AviX DFX,* Solme AB, 2017.

[19] Granta Design, "Granta Design," 2020. [Online]. Available: https://grantadesign.com/language-home/education/ces-edupack/. [Accessed 08 05 2020].

[20] M. Okereke and S. Keates, "Computational Mechanics and the Finite Element Method," in *Finite Element Applications*, Springer, Cham, 2018.

[21] M. Okereke and S. Keates, "Finite Element Mesh Generation," in *Finite Element Applications*, Springer, Cham, 2018.

[22] S. Varnam, "ANSYS Structural Mechanics," 2010. [Online]. Available: https://support.ansys.com/staticassets/ANSYS%20UK/staticassets/ANSYS%20Structural%20Mechanics.pdf. [Accessed 01 06 2020].

[23] M. K. Thompson and J. M. Thompson, "Introduction to ANSYS and Finite Element Modeling," in *ANSYS Mechanical APDL for Finite Element Analysis*, Butterworth-Heinemann, 2017.

[24] Leybold, "Fundamentals of leak detection," 01 12 2016. [Online]. Available: https://www.leyboldproducts.com/media/pdf/90/c7/87/Fundamentals_of_Leak_Detection_EN.pdf. [Accessed 01 06 2020].

[25] National Aeronautics and Space Administration, *Leak Test Requirements,* 2019.

[26] Pfeiffer Vacuum, "Desorption, diffusion, permeation and leaks," [Online]. Available: https://www.pfeiffer-vacuum.com/en/know-how/introduction-to-vacuum-technology/influences-in-real-vacuum-systems/desorption-diffusion-permeation-and-leaks/#eqn-1-35.

[27] T. Kopczynski, "Five Factors That Can Affect Your Weighing System's Accuracy," Hardy Process Solutions, San Diego, 2011.

[28] A. Pregelj and M. Drab, "LEAK DETECTION METHODS AND DEFINING THE SIZES OF LEAKS," *NDT net,* 1999.

[29] Sciemetric, "The difference between a pressure decay leak test and a mass flow leak test (and which one to use)," 01 06 2016. [Online]. Available: https://www.sciemetric.com/blog/difference-between-pressure-decay-leak-test-and-mass-flow-leak-test-and-which-one-use. [Accessed 01 06 2020].

[30] Pfeiffer Vacuum, "Mass Extraction ATC," 2020. [Online]. Available: https://www.pfeiffer-vacuum.com/en/products/leak-detection/leak-testing-ccit-solutions-for-pharma/mass-extraction-atc/. [Accessed 19 04 2020].

[31] Vacuum instruments corporation, "Comparison of Major Leak Detection Techniques," 26 04 2020. [Online]. Available: https://vicleakdetection.com/page/1062/comparison-of-major-leak-detection-techniques. [Accessed 01 06 2020].

[32] P. Cruikshank and G. Bregliozzi, "Leak Detection Tutorial," 2017.

[33] VTech, "Leak Detection Methods: A Comparative Study of Technologies and Techniques," [Online]. Available: https://cdn.thomasnet.com/ccp/20106502/32497.pdf. [Accessed 01 06 2020].

[34] Pfeiffer Vacuum, "Local Leak Detection," [Online]. Available: https://www.pfeiffer-vacuum.com/en/know-how/leak-detection/leak-detection-with-tracer-gases/local-leak-detection/. [Accessed 01 06 2020].

[35] TM Electronics, "Leak, Flow and Package testing 101," 2008. [Online]. Available: http://www.tmelectronics.com/userfiles/files/Leak-Flow-Testing-101-08232013.pdf. [Accessed 15 04 2020].

[36] I. Muller, R. Machado de Brito, C. Eduardo Pereira and V. Brusamarello, "Load cells in force sensing analysis - theory and a novel application," *IEEE Instrumentation & Measurement Magazine,* pp. 15-19, 2010.

[37] G. N. Greaves, A. L. Greer, R. S. Lakes and T. Rouxel, "Poisson's ratio and modern materials," *Nature Materials,* pp. 823-837, 2011.

[38] Encardio Rite, *Strain Gauge Principle, Types, Features and Applications,* 2019.

[39] D. Roylance, *STRESS-STRAIN CURVES,* Cambridge, Massachusetts: Department of Materials Science and Engineering, Massachusetts Institute of Technology, 2001.

[40] VPG Transducers, *Load Cells and Weigh Modules,* 2015.

[41] Futek, "Spec Sheet Futek LTH300," 2020. [Online]. Available: https://camatsystem.com/wp-content/uploads/2014/07/Datablad-lth300.pdf. [Accessed 01 06 2020].

[42] Elkome, "Futek LTH300-FSH03964," 2020. [Online]. Available: https://shop.elkome.com/en/lth300-fsh03964-donut-load-cell.html. [Accessed 01 06 2020].

[43] Camat Systems, "N320 Digital Indikator," 2020. [Online]. Available: https://camatsystem.com/produkt/n320-digital-indikator/. [Accessed 01 05 2020].

[44] PZT Application Manual, "Ltpa observer project," [Online]. Available: https://www.ltpaobserverproject.com/uploads/3/0/2/0/3020041/piezoelectric_effect_basics.pdf. [Accessed 01 06 2020].

[45] M. Valle and R. S. Dahiya, Robotic Tactile Sensing- Technologies and Sensing, Dordrecht: Springer, 2013.

[46] J. Hjelmgren, "Dynamic Measurement of Pressure - A Literature Survey," SP Technical Research Institute of Sweden, Borås, 2002.

[47] KISTLER, "SlimLine Sensors (SLS)," 2009. [Online]. Available: https://www.kistler.com/?type=669&fid=107313&model=document. [Accessed 27 04 2020].

[48] KISTLER, "Process Instrumentation and," 2012. [Online]. Available: http://sensitec.mx/pdf/manufactura.pdf. [Accessed 27 04 2020].

[49] L. E. Hollander, G. L. Vick and T. J. Diesel, "The Piezoresistive Effect and its Applications," *The Review of Scientific Instruments,* pp. 323-327, 1960.

[50] Interlink Electronics, *FSR 400 Series Data Sheet,* Camarillo, California.

[51] Interlink Electronics, *Datasheet FSR UX,* Camarillo, California, 2019.

[52] Interlink Electronics, 2020. [Online]. Available: https://buyinterlinkelectronics.com/collections/x-ux-force-sensors/products/fsr-ux-406. [Accessed 01 06 2020].

[53] TekScan, "Force Sensors," 2020. [Online]. Available: https://www.tekscan.com/force-sensors. [Accessed 01 06 2020].

[54] TekScan, *FlexiForce Standrad Model A502,* TekScan, 2019.

[55] Tekscan, "FlexiForce OEM Development Kit," 2020. [Online]. Available: https://www.tekscan.com/products-solutions/electronics/flexiforce-oem-development-kit. [Accessed 01 06 2020].

[56] Tactilus, "Off-The-Shelf Sensor Solutions," 11 08 2018. [Online]. Available: https://www.sensorprod.com/pdf/tactilus-off-the-shelf-sensor-solutions.pdf. [Accessed 01 06 2020].

[57] Sensor Products Inc., "Tactilus vs Prescale," 2020. [Online]. Available: https://www.sensorprod.com/tactilus-vs-prescale.php. [Accessed 02 05 2020].

[58] Sensor Products Inc., *Tactilus Brochure,* Madison, New Jersey: Sensor Products Inc., 2017.

[59] Z. Kappassov, V. Perdereau and J. A. C. Ramon, "Tactile sensing in dexterous robot hands," *Robotics and Autonomous Systems,* 2015.

[60] Pressure Profile Systems, "Industrial TactArray," 2019. [Online]. Available: https://pressureprofile.com/tactarray/industrial-tactarray. [Accessed 01 06 2020].

[61] Pressure Profile Systems, *Industrial TactArray System Spec Sheet,* 2014.

[62] SensorProd, "Pressurex micro green brochure," 30 10 2014. [Online]. Available: https://www.sensorprod.com/pdf/pressurex-micro-green-brochure.php. [Accessed 01 06 2020].

[63] SensorProd, "Pressurex Micro Green Pricing," 28 10 2014. [Online]. Available: https://www.sensorprod.com/pdf/pressurex-micro-green-pricing.pdf. [Accessed 01 06 2020].

[64] Tekscan, "Tactile Pressure Sensor Solutions," [Online]. Available: https://www.tekscan.com/tactile-pressure-sensors. [Accessed 01 06 2020].

[65] Tekscan, "Pressure Mapping Sensor 5051," 02 02 2015. [Online]. Available: https://www.tekscan.com/products-solutions/pressure-mapping-sensors/5051. [Accessed 01 06 2020].

[66] TekScan, *I-Scan Product Selection Guide,* 2020.

[67] M. Shigyo.USA Patent 6564641 B1, 2003.

[68] Fujifilm, "Pressure Measurment Film - Prescale," [Online]. Available: https://camatsystem.com/wp-content/uploads/2014/11/Datablad-PRESCALE.pdf. [Accessed 01 06 2020].

[69] Camat Systems, "Fujifilm Prescale," [Online]. Available: https://camatsystem.com/produkt/fujifilm-prescale/. [Accessed 01 06 2020].

[70] SensorProd, "Surface Profiler Film Brochure," 27 01 2014. [Online]. Available: https://www.sensorprod.com/surface-profiler-film/PDFs/SPF-Brochure.pdf. [Accessed 01 06 2020].

[71] SensorProd, "Surface Profiler Film Sheet," 27 06 2014. [Online]. Available: https://www.sensorprod.com/surface-profiler-film/PDFs/SPF-Price-Sheet.pdf. [Accessed 01 06 2020].

Appendices

A: Product requirements specification

Criteria	***Goal value***	***R/W***	***Verification method***
1. Performance			
1.2 Interface surface contact	Prototype interface > current product interface (Percentage of area of zero pressure)	R	Prototype testing with chosen pressure test method
1.2 Interface Force	1400+-600 N	R	Prototype testing with chosen force test method
1.3 Leakage rate	≤ 5 ml/min	R	-
2. Design			
2.3 Modularity	Redesigned components shall fit with current antenna interface	R	-
2.3 Securing mechanism	Design shall allow for Cross-tightening / Simultaneous tightening	R	-
3. Installation & maintenance			
3.1 Installation time	≤ 14 s (Current design)	W	DFA analysis in AviX
3.2 Installation tools	Can be assembled only using standard tools	R	-

Requirements and wishes are marked with R and W respectively

B: Torque tests

10 Nm	Force in Waveguide interface, without O-ring (N)		**14 Nm**	Force in Waveguide interface, without O-ring (N)		**18 Nm**	Force in Waveguide interface, without O-ring (N)
Test 1	1630		Test 1	1667		Test 1	1721
Test 2	1670		Test 2	1735		Test 2	1644
Test 3	1694		Test 3	1685		Test 3	1618
Mean	1665		Mean	1696		Mean	1661

10 Nm	Force in Waveguide interface, with O-ring (N)		**14 Nm**	Force in Waveguide interface, with O-ring (N)		**18 Nm**	Force in Waveguide interface, with O-ring (N)
Test 1	1350		Test 1	1405		Test 1	1515
Test 2	1376		Test 2	1379		Test 2	1479
Test 3	1429		Test 3	1335		Test 3	1375
Mean	1385		Mean	1373		Mean	1456

C: Fuji Film contact test

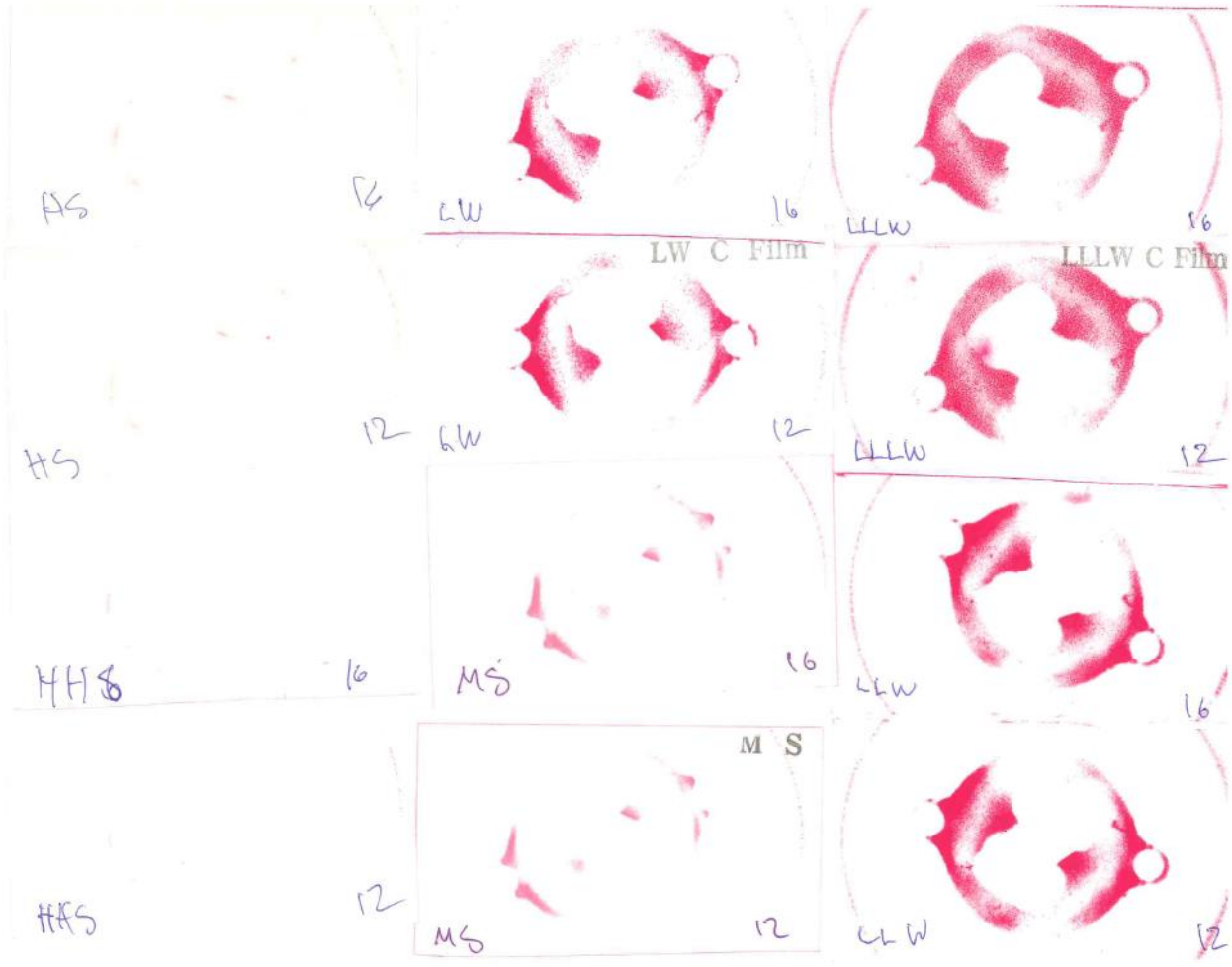

D: Contact pressure simulation tests with two, three and four attachment points

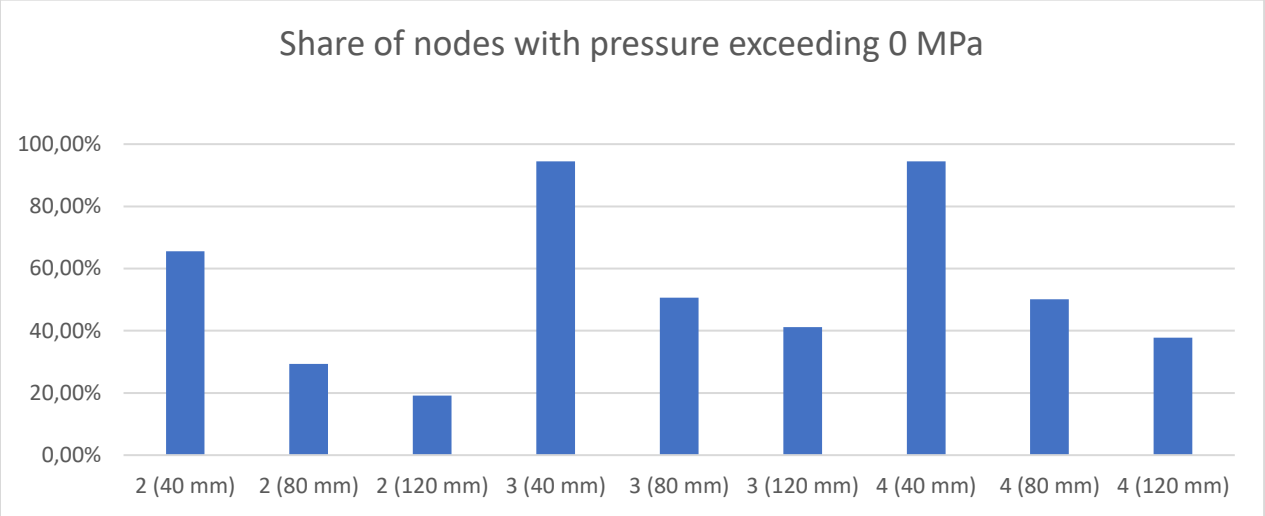

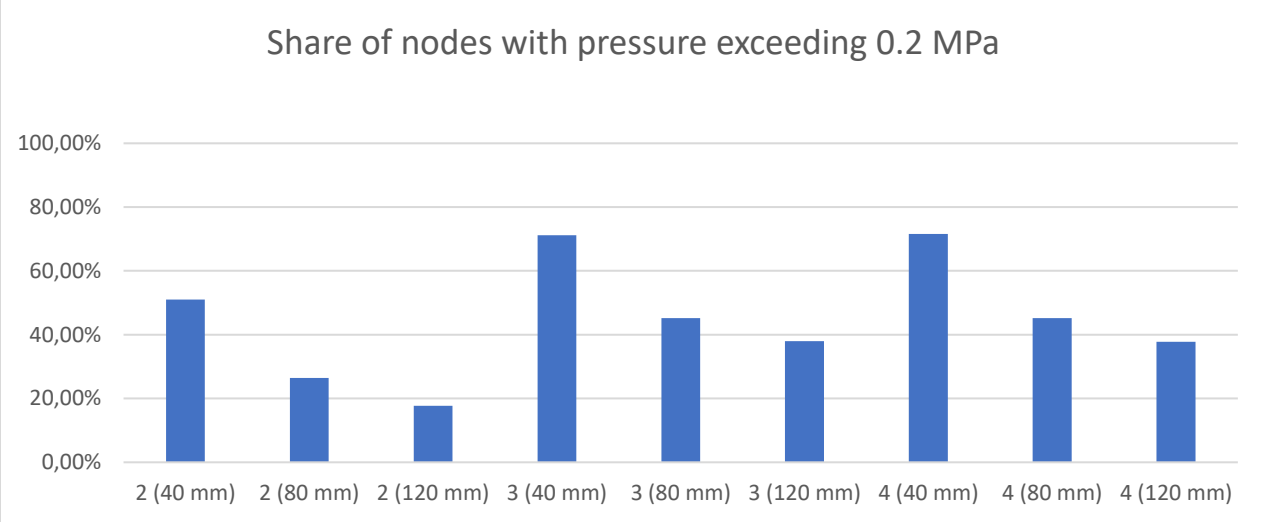

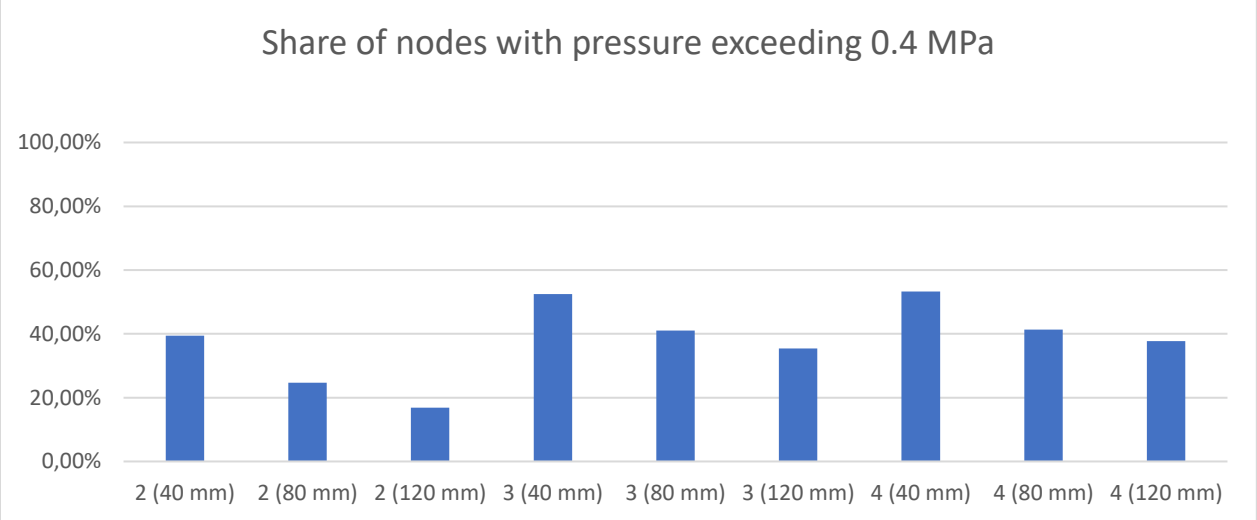

E: Contact pressure simulation tests with three contacts points and current design

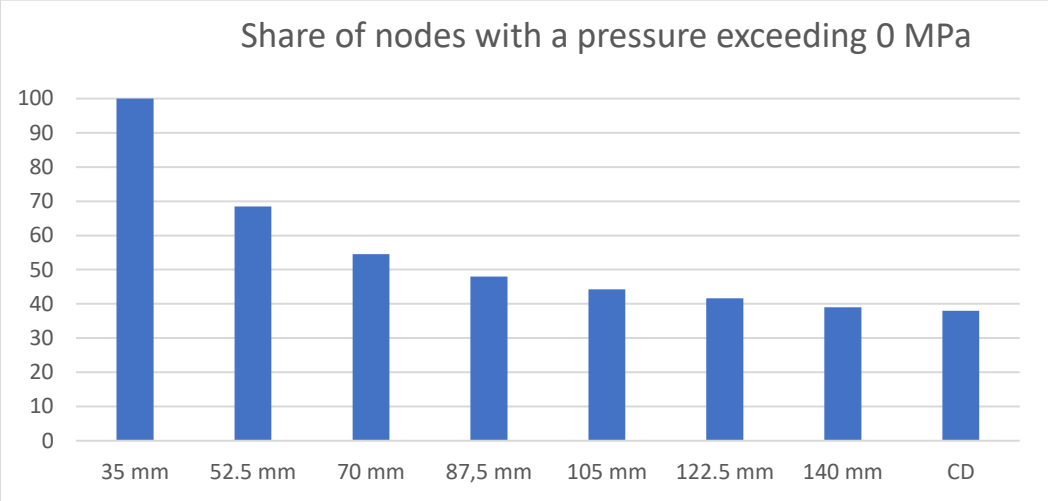

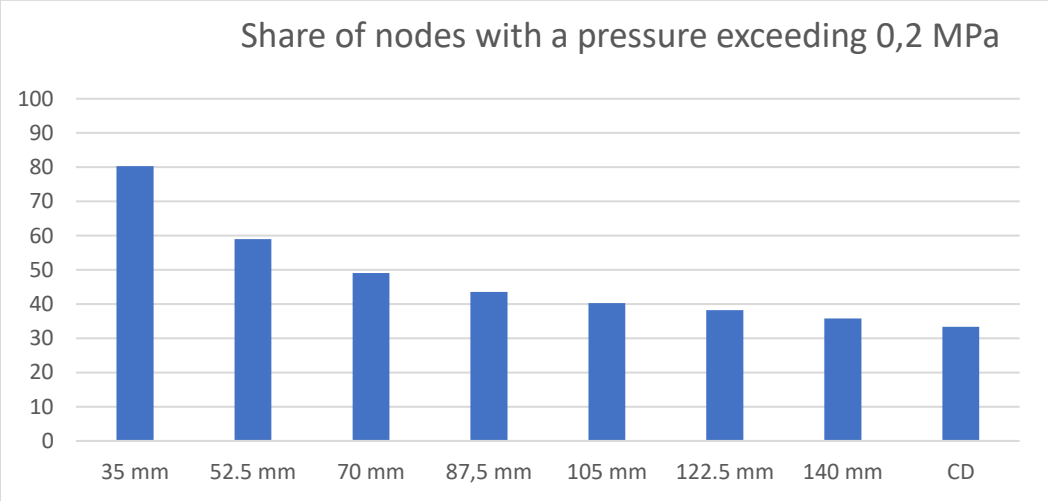

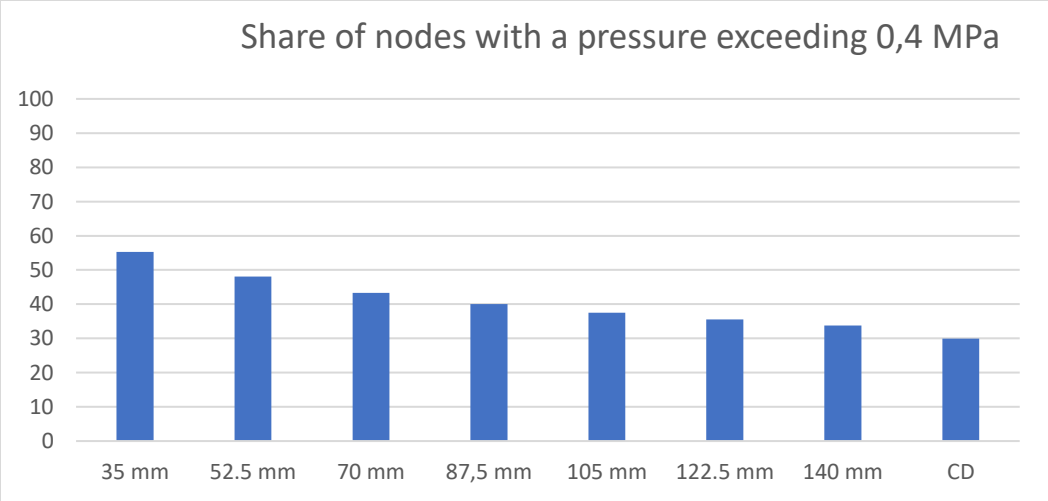

Weight Case 1

	Weight:		1	Weight:		5	Weight:		3	Weight:		1		
	In-house assembly process (lower is better)			**At site assembly process (lower is better)**			**Manufactuing cost (lower is better)**			**Component cost (lower is better)**			**Requirements**	(Y=YES, N=NO)
	Assembly Time	Score	Weighted Score	Assembly Time	Score	Weighted Score	Man. score	Score	Weighted Score	Cost score	Score	Weighted Score	Standard tools	Cross-tightening / Simultaneous tightening
Camlock 1 (3)	153,2	20	20	21,2	11	55	55	20	60	0	0	0	Y	N
Camlock 2 (4)	105,1	14	14	27,2	15	75	36	13	39	0	0	0	Y	Y
CPU	72,9	10	10	18,5	10	50	51	19	57	0	0	0	Y	Y
Deforming plate 1 (1)	62,2	8	8	13,9	7	35	49	18	54	0	0	0	Y	Y
Deforming plate 2 (2)	63,9	8	8	15,6	8	40	49	18	54	0	0	0	Y	Y
Screw Cap	85,1	11	11	16	9	45	31	11	33	6	17	17	N	Y
Spring loaded Screws 1 (3)	92,6	12	12	35,6	19	95	44	16	48	1	3	3	Y	N
Spring loaded Screws 2 (4)	92,8	12	12	28,3	15	75	44	16	48	1	3	3	Y	Y
Toggle latches 1 (3)	107,3	14	14	30,5	16	80	31	11	33	1	3	3	Y	N
Toggle latches 2 (4)	113,9	15	15	27,5	15	75	31	11	33	2	6	6	Y	Y
Tri-Connector	56	7	7	24,5	13	65	32	12	36	7	20	20	Y	Y
Wedges 1 (3)	88,7	12	12	31,1	17	85	50	18	54	0	0	0	Y	N
Wedges 2 (4)	101,1	13	13	37,3	20	100	50	18	54	0	0	0	Y	Y
Scaling factor:	7,66			1,865			2,75			0,35				
Converts cost scores / assembly times to a score between 0-20														

Total score (lower is better)	**Total Weighted score (lower is better)**				**Top Five Concepts:**
51	135	Camlock 1 (3)	Does not fulfill requirements	1	Deforming plate 1 (1)
42	128	Camlock 2 (4)	Fulfills requirements	2	Deforming plate 2 (2)
39	117	CPU	Fulfills requirements	3	Screw Cap
33	97	Deforming plate 1 (1)	Fulfills requirements	4	CPU
34	102	Deforming plate 2 (2)	Fulfills requirements	5	Tri-connector
48	106	Screw Cap	Does not fulfill requirements		
50	158	Spring loaded Screws 1 (3)	Does not fulfill requirements		
46	138	Spring loaded Screws 2 (4)	Fulfills requirements		
44	130	Toggle latches 1 (3)	Does not fulfill requirements		
47	129	Toggle latches 2 (4)	Fulfills requirements		
52	128	Tri-Connector	Fulfills requirements		
47	151	Wedges 1 (3)	Does not fulfill requirements		
51	167	Wedges 2 (4)	Fulfills requirements		

Weight Case 2

	Weight:	1		Weight:	5		Weight:	3		Weight:	2			
	In-house assembly process (lower is better)			**At site assembly process (lower is better)**			**Manufactuing cost (lower is better)**			**Component cost (lower is better)**			**Requirements**	
	Assembly Time	Score	Weighted Score	Assembly Time	Score	Weighted Score	Man. score	Score	Weighted Score	Cost score	Score	Weighted Score	Standard tools	Cross-tightening / Simultaneous tightening
Camlock 1 (3)	153,2	20	20	21,2	11	55	55	20	60	0	0	0	Y	N
Camlock 2 (4)	105,1	14	14	27,2	15	75	36	13	39	0	0	0	Y	Y
CPU	72,9	10	10	18,5	10	50	51	19	57	0	0	0	Y	Y
Deforming plate 1 (1)	62,2	8	8	13,9	7	35	49	18	54	0	0	0	Y	Y
Deforming plate 2 (2)	63,9	8	8	15,6	8	40	49	18	54	0	0	0	Y	Y
Screw Cap	85,1	11	11	16	9	45	31	11	33	6	17	34	N	Y
Spring loaded Screws 1 (3)	92,6	12	12	35,6	19	95	44	16	48	1	3	6	Y	N
Spring loaded Screws 2 (4)	92,8	12	12	28,3	15	75	44	16	48	1	3	6	Y	Y
Toggle latches 1 (3)	107,3	14	14	30,5	16	80	31	11	33	1	3	6	Y	N
Toggle latches 2 (4)	113,9	15	15	27,5	15	75	31	11	33	2	6	12	Y	Y
Tri-Connector	56	7	7	24,5	13	65	32	12	36	7	20	40	Y	Y
Wedges 1 (3)	88,7	12	12	31,1	17	85	50	18	54	0	0	0	Y	N
Wedges 2 (4)	101,1	13	13	37,3	20	100	50	18	54	0	0	0	Y	Y
Scaling factor:	7,66			1,865			2,75			0,35				
Converts cost scores / assembly times to a score between 0-20														

Total score (lower is better)	**Total Weighted score (lower is better)**				**Top Five Concepts:**
51	135	Camlock 1 (3)	Does not fulfill requirements	1	Deforming plate 1 (1)
42	128	Camlock 2 (4)	Fulfills requirements	2	Deforming plate 2 (2)
39	117	CPU	Fulfills requirements	3	CPU
33	97	Deforming plate 1 (1)	Fulfills requirements	4	Screw Cap
34	102	Deforming plate 2 (2)	Fulfills requirements	5	Camlock 2 (4)
48	123	Screw Cap	Does not fulfill requirements		
50	161	Spring loaded Screws 1 (3)	Does not fulfill requirements		
46	141	Spring loaded Screws 2 (4)	Fulfills requirements		
44	133	Toggle latches 1 (3)	Does not fulfill requirements		
47	135	Toggle latches 2 (4)	Fulfills requirements		
52	148	Tri-Connector	Fulfills requirements		
47	151	Wedges 1 (3)	Does not fulfill requirements		
51	167	Wedges 2 (4)	Fulfills requirements		

Weight Case 3

	Weight: 1			Weight: 5			Weight: 4			Weight: 1				
	In-house assembly process (lower is better)			**At site assembly process (lower is better)**			**Manufactuing cost (lower is better)**			**Component cost (lower is better)**			**Requirements**	
	Assembly Time	Score	Weighted Score	Assembly Time	Score	Weighted Score	Man. score	Score	Weighted Score	Cost score	Score	Weighted Score	Standard tools	Cross-tightening / Simultaneous tightening
Camlock 1 (3)	153,2	20	20	21,2	11	55	55	20	80	0	0	0	Y	N
Camlock 2 (4)	105,1	14	14	27,2	15	75	36	13	52	0	0	0	Y	Y
CPU	72,9	10	10	18,5	10	50	51	19	76	0	0	0	Y	Y
Deforming plate 1 (1)	62,2	8	8	13,9	7	35	49	18	72	0	0	0	Y	Y
Deforming plate 2 (2)	63,9	8	8	15,6	8	40	49	18	72	0	0	0	Y	Y
Screw Cap	85,1	11	11	16	9	45	31	11	44	6	17	17	N	Y
Spring loaded Screws 1 (3)	92,6	12	12	35,6	19	95	44	16	64	1	3	3	Y	N
Spring loaded Screws 2 (4)	92,8	12	12	28,3	15	75	44	16	64	1	3	3	Y	Y
Toggle latches 1 (3)	107,3	14	14	30,5	16	80	31	11	44	1	3	3	Y	N
Toggle latches 2 (4)	113,9	15	15	27,5	15	75	31	11	44	2	6	6	Y	Y
Tri-Connector	56	7	7	24,5	13	65	32	12	48	7	20	20	Y	Y
Wedges 1 (3)	88,7	12	12	31,1	17	85	50	18	72	0	0	0	Y	N
Wedges 2 (4)	101,1	13	13	37,3	20	100	50	18	72	0	0	0	Y	Y

Scaling factor:	7,66	1,865	2,75	0,35
Converts cost scores / assembly times to a score between 0-20				

Total score (lower is better)	**Total Weighted score (lower is better)**				**Top Five Concepts:**
51	155	Camlock 1 (3)	Does not fulfill requirements	1	Deforming plate 1 (1)
42	141	Camlock 2 (4)	Fulfills requirements	2	Screw Cap
39	136	CPU	Fulfills requirements	3	Deforming plate 2 (2)
33	115	Deforming plate 1 (1)	Fulfills requirements	4	CPU
34	120	Deforming plate 2 (2)	Fulfills requirements	5	Toggle latches 2 (4)
48	117	Screw Cap	Does not fulfill requirements		
50	174	Spring loaded Screws 1 (3)	Does not fulfill requirements		
46	154	Spring loaded Screws 2 (4)	Fulfills requirements		
44	141	Toggle latches 1 (3)	Does not fulfill requirements		
47	140	Toggle latches 2 (4)	Fulfills requirements		
52	140	Tri-Connector	Fulfills requirements		
47	169	Wedges 1 (3)	Does not fulfill requirements		
51	185	Wedges 2 (4)	Fulfills requirements		

Weight Case 4

	Weight: 1			Weight: 5			Weight: 4			Weight: 2				
	In-house assembly process (lower is better)			**At site assembly process (lower is better)**			**Manufactuing cost (lower is better)**			**Component cost (lower is better)**			**Requirements**	
	Assembly Time	Score	Weighted Score	Assembly Time	Score	Weighted Score	Man. score	Score	Weighted Score	Cost score	Score	Weighted Score	Standard tools	Cross-tightening / Simultaneous tightening
Camlock 1 (3)	153,2	20	0	21,2	11	55	55	20	80	0	0	0	Y	N
Camlock 2 (4)	105,1	14	14	27,2	15	75	36	13	52	0	0	0	Y	Y
CPU	72,9	10	10	18,5	10	50	51	19	76	0	0	0	Y	Y
Deforming plate 1 (1)	62,2	8	8	13,9	7	35	49	18	72	0	0	0	Y	Y
Deforming plate 2 (2)	63,9	8	8	15,6	8	40	49	18	72	0	0	0	Y	Y
Screw Cap	85,1	11	11	16	9	45	31	11	44	6	17	34	N	Y
Spring loaded Screws 1 (3)	92,6	12	12	35,6	19	95	44	16	64	1	3	6	Y	N
Spring loaded Screws 2 (4)	92,8	12	12	28,3	15	75	44	16	64	1	3	6	Y	Y
Toggle latches 1 (3)	107,3	14	14	30,5	16	80	31	11	44	1	3	6	Y	N
Toggle latches 2 (4)	113,9	15	15	27,5	15	75	31	11	44	2	6	12	Y	Y
Tri-Connector	56	7	7	24,5	13	65	32	12	48	7	20	40	Y	Y
Wedges 1 (3)	88,7	12	12	31,1	17	85	50	18	72	0	0	0	Y	N
Wedges 2 (4)	101,1	13	13	37,3	20	100	50	18	72	0	0	0	Y	Y
Scaling factor:	7,66			1,865			2,75			0,35				
Converts cost scores / assembly times to a score between 0-20														

Total score (lower is better)	**Total Weighted score (lower is better)**				**Top Five Concepts:**
51	135	Camlock 1 (3)	Does not fulfill requirements	1	Deforming plate 1 (1)
42	141	Camlock 2 (4)	Fulfills requirements	2	Deforming plate 2 (2)
39	136	CPU	Fulfills requirements	3	Screw Cap
33	115	Deforming plate 1 (1)	Fulfills requirements	4	CPU
34	120	Deforming plate 2 (2)	Fulfills requirements	5	Camlock 2 (4)
48	134	Screw Cap	Does not fulfill requirements		
50	177	Spring loaded Screws 1 (3)	Does not fulfill requirements		
46	157	Spring loaded Screws 2 (4)	Fulfills requirements		
44	144	Toggle latches 1 (3)	Does not fulfill requirements		
47	146	Toggle latches 2 (4)	Fulfills requirements		
52	160	Tri-Connector	Fulfills requirements		
47	169	Wedges 1 (3)	Does not fulfill requirements		
51	185	Wedges 2 (4)	Fulfills requirements		

G: Contact pressure test of prototype with Fujifilm Prescale (LLLW)

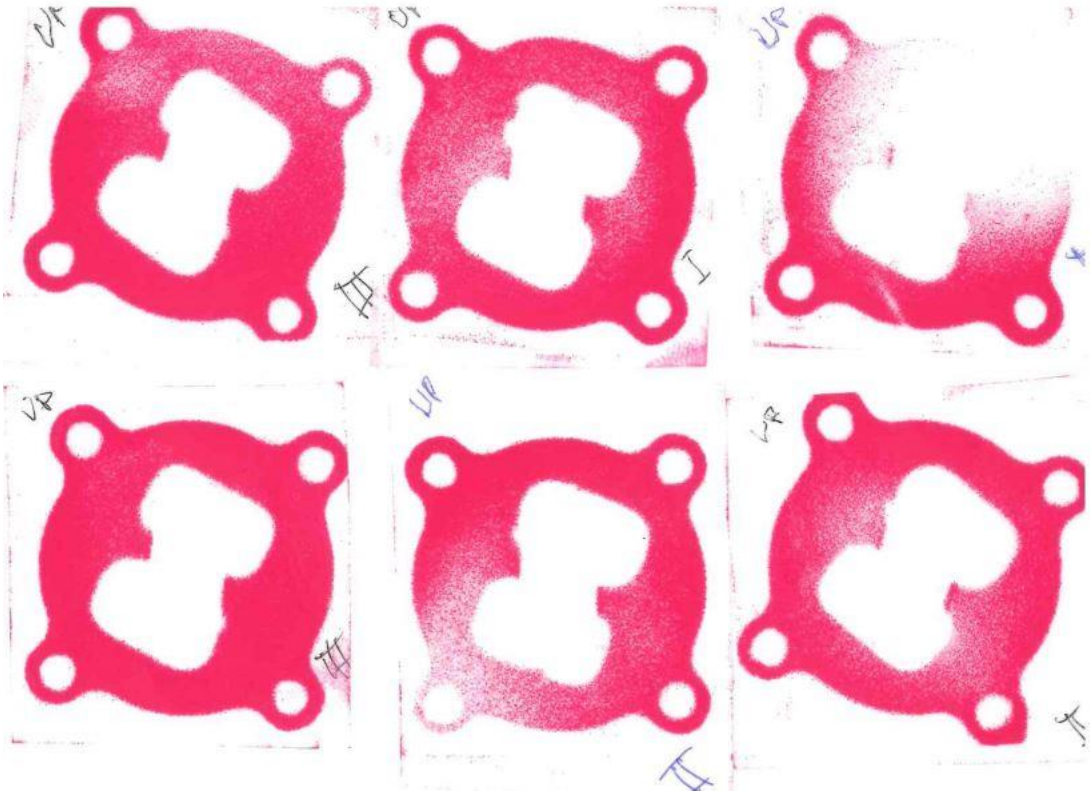

DEPARTMENT OF INDUSTRIAL AND MATERIALS SCIENCE
CHALMERS UNIVERSITY OF TECHNOLOGY
Gothenburg, Sweden
www.chalmers.se

CHALMERS
UNIVERSITY OF TECHNOLOGY